Stable carbon and hydrogen isotope fractionation of volatile organic compounds caused by vapor-liquid equilibrium

Daniel Bouchard, Patrick H hener, Didier Gori, Daniel Hunkeler, Tim Buscheck

Stable carbon and hydrogen isotope fractionation of volatile organic compounds caused by vapor-liquid equilibrium

Daniel Bouchard[1,2*], Patrick Höhener[3], Didier Gori[3], Daniel Hunkeler[2] and Tim Buscheck[4]

Chemosphere

[1]Contam-i-sotopes, inc.
1613 Rue du Verger,
St-Bruno, Qc, Canada.
Contam-i-sotopes@outlook.com

[2]Centre for Hydrogeology and Geothermics (CHYN)
University of Neuchâtel,
Rue Emile Argand 11
CH-2000 Neuchâtel, Switzerland

[3]Aix Marseille University – CNRS, UMR 7376,
Laboratory of Environmental Chemistry, 3 place Victor Hugo, F-13331 Marseille, France

[4]Chevron Technical Center
6001 Bollinger Canyon Road
San Ramon, CA, USA 94583

*Corresponding author

Abstract

Several types of laboratory experiments were conducted to evaluate isotope fractionation caused by phase transfer process for a selection of common environmental contaminants. Carbon and hydrogen isotope fractionation caused by vaporization of non-aqueous phase liquid (NAPL), by volatilization from water and by dissolution into an organic solvent (tetraethylene glycol dimethylether or TGDE) was investigated under closed system experimental setups to isolate the air-liquid partitioning process. A selection of aromatic, aliphatic and chlorinated compounds along with one fuel oxygenate (methyl tert-butyl ether or MTBE) were evaluated to determine isotope the enrichment factor related to respective phase transfer process. During NAPL vaporization, the residual mass of aromatic compounds, aliphatic compounds and MTBE became progressively depleted in heavy carbon and hydrogen isotopes. In contrast, during volatilization from water, the residual mass of aromatic compounds and MTBE dissolved in the water became progressively enriched in heavy hydrogen isotopes, whereas no significant change in carbon isotope was observed, except for MTBE showing a significant depletion. For the air-TGDE partitioning process, most of the aromatic compounds tested led to no significant carbon (except ethylbenzene) or hydrogen (except toluene and *o*-xylene) isotope fractionation. In contrast, significant carbon isotope fractionation was observed for aliphatic and chlorinated compounds and hydrogen isotope fractionation for aliphatic compounds, and are comparable to progressive NAPL vaporization in direction and magnitude. The isotope fractionation factors determined in this study are key for interpreting the change in isotope ratios when assessing the fate of gas-phase VOCs present in the soil air or when gas-phase VOCs are sampled using TGDE as the sink matrix. The results of this study contribute to expand the list of common environmental contaminants that can be assessed by the compound-specific isotope analysis (CSIA) method deployed in the frame of gas-phase studies.

Keywords: Stable isotopes, carbon isotope, hydrogen isotope, VOC volatilization, organic liquid vaporization, isotope fractionation.

1. Introduction

Volatile organic compounds (VOCs) represent an important class of subsurface environmental contaminants, among which chlorinated solvents and petroleum hydrocarbons are commonly encountered. In general, these contaminants have penetrated into the subsurface as non-aqueous phase liquids (NAPL) due to accidental releases above ground or improper storage tank containment in the subsurface. During downward migration through the unsaturated zone, portions of the moving NAPL become immobilized in the soil pores, resulting in a residual saturation ranging from 2 to 20% of the soil pore volume (Boulding, 1995). Due to their high vapor pressure, VOCs are expected to volatilize from the immobilized NAPL and migrate by gas-phase diffusion through the soil porosity, thus forming gas-phase plumes. potentially posing threats to human health if entering buildings (so called vapor intrusion process) (Johnson and Ettinger, 1991; Verginelli et al., 2016) or contaminating sub laying groundwater resources (Grathwohl et al., 2003). Biodegradation and chemical oxidation are naturally occurring attenuation processes limiting gas-phase plume expansion by transforming VOCs into less harmful compounds (see Rivett et al. (2011) for an extensive review of processes). Aerobic biodegradation of VOCs during migration can be expected to readily occur for petroleum hydrocarbons under field conditions (Lahvis et al., 1999; Baker et al., 2000; Christophersen et al., 2005; Davis et al., 2005; Höhener et al., 2006; Molins et al., 2010; Sihota et al., 2016). Aerobic biodegradation of chlorinated compounds in the unsaturated zone may also naturally occur, with biodegradation of *cis*-DCE and VC being commonly reported (Kirtland et al., 2003; Patterson et al., 2013; Kurt et al., 2014). The literature remains scarce regarding aerobic biodegradation of TCE. While shown to occur in aqueous media (Barth et al., 2002; Chu et al., 2004; Clingenpeel et al., 2012), occurrence during gas-phase transport in unsaturated soil remains to be demonstrated. Similarly, chemical oxidation of TCE under oxic conditions was shown to occur in aqueous media (Pham et al., 2008; Schaefer et al., 2018), but occurrence during gas-phase transport in unsaturated soil also remains to be validated. Finally, anoxic environments favorable to anaerobic biodegradation can also

89 be developed at sites where the oxygen is consumed at higher rates than supplying rates (Molins et
90 al., 2010), which was also shown to contribute limiting petroleum hydrocarbon plume expenditure.
91
92 Natural source zone depletion (NSZD) by physical and reactive processes has been presented as a
93 viable site management strategy (Johnson et al., 2013). Relying on natural attenuation processes as a
94 site management strategy is acceptable when one can scientifically document the occurrence and
95 contribution of attenuation processes along with quantification of contaminant mass reduction rates,
96 while posing no risk to nearby population or natural resources. Quantification of mass reduction
97 rates associated with a source zone located in the unsaturated zone is generally carried out by
98 evaluating concentration changes for each targeted VOC in the soil gas over time (Cozzarelli et al.,
99 2001; Lundegard and Johnson, 2006). However, understanding the VOC mass-transfer dynamics of a
100 multiple-component NAPL is critical to accurately assess fate and contaminant transport, and yet
101 represents a challenge to predict (Wang et al., 2003; Broholm et al., 2005; McColl et al., 2008). In
102 addition, while VOC concentrations are dependent on many environmental factors (for instance
103 seasonal temperature variation, recharge water or groundwater level fluctuation), representative
104 concentrations over space and time remain a limiting factor in quantifying accurate NSZD rates
105 (Ponsin et al., 2015; Sihota et al., 2016). When remediation actions on the source are required, some
106 engineered systems will take advantage of the high vapor pressure of the contaminants to accelerate
107 source mass reduction. Soil vapor extraction (SVE) systems were shown to be an effective method for
108 removing VOCs from the unsaturated zone, and thus became a common technology deployed by
109 remediation engineers. Over prolonged treatment duration, the treatment efficiency tends to
110 decrease indicated by reduced mass-removal rates and concentration tailings. This efficiency loss is
111 caused by different physical, chemical, and biological factors influencing contaminant transport
112 (McColl et al., 2008), from which emerges the question whether or not the treatment efficiency
113 reached its limitations and should thus be ended. To confidently determine proper NSZD rates in the
114 unsaturated zones or to appropriately evaluate the efficiency of remediation systems applied to

unsaturated zones, field practitioners therefore need assessment tools that are suitable for gas-phase investigations.

Compound-Specific Isotope Analysis (CSIA) is a process-specific assessment tool increasingly used in gas-phase studies. CSIA was shown to be an appropriate assessment tool to evaluate NSZD in the unsaturated zone (Bouchard et al., 2008b; Höhener et al., 2008; Bouchard et al., 2011), to assess for vapor intrusion (McHugh et al., 2011; Jeannottat and Hunkeler, 2013; Beckley et al., 2016) and to evaluate the performance of remediation systems (Bouchard et al., 2017a; Bouchard et al., 2018b; Zamane et al., 2020). Basically, the CSIA method aims at tracking the isotope ratio evolution of an element ($^{13}C/^{12}C$, $^{2}H/^{1}H$, $^{37}Cl/^{35}Cl$) for selected VOC with time (and/or distance) to demonstrate VOC biodegradation (Aelion et al., 2010) or to identify the dominant attenuation process (Kuder et al., 2009; Bouchard et al., 2018a). The impact of biodegradation on the isotopic composition of VOC is well understood and leads to an accumulation of heavy isotopes (i.e. isotope enrichment) in the remaining pool of VOCs due to slower reaction kinetics of molecules including a heavy isotope. However, it was shown that some physical attenuation processes, which had been neglected when applying CSIA for VOCs in saturated soil conditions (i.e. groundwater), must be considered in unsaturated soil conditions as causing significant isotope fractionation. For instance, vaporization of organic liquid, air-water partitioning and gaseous diffusion are physical processes known to change the isotopic composition of gas-phase VOCs (Bouchard et al., 2008b; Kuder et al., 2009). These processes are hence expected to impact the isotopic signature of the VOCs during the course of passive vaporization (such as during natural source zone depletion) or during an active engineered remediation treatment. The direction (i.e. enrichment or depletion in heavy isotopes) and the magnitude of the isotope fractionation is, however, dependent on the conditions under which the processes are occurring. For equilibrium conditions in a closed system (i.e. static conditions), an isotope fractionation is expected due to different vapor pressure properties for isotopically different molecules (and called isotopologues) (Van Hook, 2006; Wolfsberg et al., 2010). In contrast, for non-

equilibrium conditions in an open system (i.e. dynamic conditions), isotope fractionation due to kinetic processes such as gaseous and aqueous diffusion is occurring, and the observed isotopic change reflecting the processes interplay (vapor pressure and diffusion) is explained by the Craig-Gordon model (Kuder et al., 2009; Jeannottat and Hunkeler, 2012; Julien et al., 2015b; Kopinke and Georgi, 2017). Currently, the direction and the magnitude of the isotope fractionation caused by vaporization and air-water partitioning process (under equilibrium conditions) are known for only few VOCs and elements, which limits the number of VOCs that can be assessed on field sites.

Lastly, application of CSIA in gas-phase studies is still largely limited due to lack of appropriate sampling devices specific to isotope measurements. A simple and robust solvent-based method specifically developed to facilitate isotope measurement on collected gas-phase VOCs has been recently documented as an alternative sampling method (Bouchard et al., submitted). The method uses tetraethylene glycol dimethylether (TGDE) as a liquid sink matrix to accumulate the gaseous VOCs. TGDE was selected among other potential solvents due to its lower vapor pressure property, increased affinity with polar and apolar compounds, and lastly due to absence of interference with the analytes during the analytical measurements (Bouchard et al., 2017b). During the sampling process, dissolution of gas-phase VOC into TGDE is controlled by the air-solvent partitioning process. This air-solvent partitioning process potentially leads to an isotope fractionation during the sampling process, which warrants further evaluations.

This study has two objectives, both focusing on isotope fractionation caused by phase transfer processes. First, carbon and hydrogen isotope fractionation factors related to vaporization from organic liquid and air-water partitioning under equilibrium conditions were determined for a selection of aromatic, aliphatic and fuel oxygenate compounds. A large subset of hydrocarbons was tested to evaluate the isotope fractionation variability related to different molecular structure, and in view to expand the CSIA application in soil gas studies to additional common contaminants observed

at contaminated sites. Second, with the aim to support the development of the solvent-based sampling method specific to CSIA, carbon and hydrogen isotope fractionation related to air-TGDE partitioning was evaluated for a selection of aromatic, aliphatic, fuel oxygenate and chlorinated compounds. An isotope-specific analytical simulation was subsequently conducted reproducing the progressive accumulation of VOCs into TGDE during a sampling event. The analytical simulation was performed with the purpose of gaining comprehensive insights on the isotope fractionation caused by air-TGDE partitioning process during transient and steady state conditions.

2. Material & methods

2.1. Laboratory experiments

2.1.1. Stepwise NAPL vaporization in closed system

Multi stepwise NAPL vaporization experiments were carried out as previously performed for chlorinated ethenes by Jeannottat and Hunkeler (2012) to quantify carbon and hydrogen isotope fractionation factor for benzene (B), toluene (T), *o*-xylene (*o*-X), cyclopentane, *n*-octane, 2,2,4-trimethylpentane (isooctane) and methyl tert-butyl ether (MTBE) (99% purity, various suppliers). The experimental setup consisted of two 5 mL air-tight syringes (Hamilton – model 1005 RN SYR for screw RN nut end tip) connected using a custom-designed screwing metal connector and maintained in vertical position during the experiment. A small 25 μL metal receptacle was welded on the lower syringe plunger to contain the NAPL. Once spiked in the receptacle, the NAPL was allowed to equilibrate (20 minutes) with a fixed volume of air inside the lower syringe only by keeping the lock closed. The selected air volume was the smaller, the higher the VOC vapor pressure. The lock was reopened, and the headspace of the lower syringe was then transferred into the upper syringe. Once the syringes disconnected, clean air was reintroduced in the lower syringe whereas isotope analysis for the gas-phase compound contained in the upper syringe was performed. The VOC mass removed per step was related to the syringe volume and the vapor pressure of the compound at the experimental temperature (25°C). The mass removal evolution was tracked by using the total

integrated peak area obtained during each isotopic analysis (see further explanation in Supplementary material). Repeated equilibration and dispense steps were performed until >95% of the NAPL mass was depleted, except for MTBE (>88%). Each compound was individually tested. For each VOC, carbon and hydrogen isotopes were evaluated separately respectively in duplicate and in triplicate experiments.

2.1.2. Stepwise air-water partitioning in closed system

Multi stepwise air-water partitioning experiments were carried out as previously performed for chlorinated ethenes by Jeannottat and Hunkeler (2012) to quantify carbon and hydrogen isotope fractionation factor for BT*o*-X and MBTE. An aqueous solution of 10 mg/L was separately prepared for each VOC in a 250 mL glass vial. Ten (10) mL of the solution was introduced into a 25 mL gas-tight glass syringe with the plunger fully extended to the 25 mL mark, hence leaving 15 mL of headspace. The syringe was closed and was slightly shaken (200 rpm) for at least 20 minutes to reach the air-water equilibrium. The headspace was dispensed in a fume hood and followed by the introduction of 15 mL of ambient air in the syringe. The equilibration-dispense step was repeated until a defined mass proportion was removed based on Henry's law (at room temperature). The relative VOC mass decrease over time was validated by concentration analysis carried out on each aqueous sample. One experimental series involved six (6) independently produced water samples with increasing number of equilibration steps. Three series were conducted for each compound (individually tested), except for MTBE (2 series). Isotope analyses were performed on the water samples in duplicates.

2.1.3. Air-TGDE partitioning in closed system

Single step air-TGDE partitioning experiments were carried out to quantify carbon and hydrogen isotope fractionation factor for a selection of aromatic compounds (BT*o*-X, ethylbenzene (E) and *m,p*-xylene (*m,p*-X)), aliphatic compounds (cyclopentane, *n*-hexane and *n*-octane) and one fuel oxygenate compound (MTBE). In addition, a selection of chlorinated compounds including perchloroethene

(PCE), trichloroethene (TCE), 1,1,2-trichloroethane (1,1,2-TCA), *cis* 1,2-dichloroethene (*cis*-DCE) and 1,2-dichloroethane (1,2-DCA) were evaluated to quantify carbon isotope fractionation factor. TGDE was obtained from Sigma-Aldrich (>99% purity) whereas the chlorinated compounds were obtained from various suppliers (all > 99 %). One (1) mL of TGDE was pipetted into a 20 mL glass vial. A defined volume of one pure compound was pipetted into the vial containing TGDE and then closed with teflon-lined septa using screw caps. The volumes were chosen according to the air-tetraglyme partitioning constant to produce about equal concentrations of each element C or H in the headspace. Additional vials without TGDE and reduced NAPL volume were prepared to measure the isotope ratio of the neat material (Table 1), again adjusting the amount of C and H to about equal vapor concentrations. These concentrations produced peaks within the IRMS linear range calibration, with amplitudes equal to reference gas peaks. For each VOC, a set of 5 vials with and without TGDE was prepared and left to equilibrate for 24 hours at 30°C. Carbon and hydrogen isotopes were evaluated in separate experiments.

Table 1: Volume of NAPL added per 20 mL vial containing TGDE (1 000 µL) or without TGDE, for each VOC tested.

Compound	With TGDE (µL)		Without TGDE (µL)	
	For ^{13}C analysis	For ^{2}H analysis	For ^{13}C analysis	For ^{2}H analysis
Benzene	20	158	0.5	0.5
Toluene	34	269	0.5	0.5
Ethylbenzene	115	462	1	1
m,p-xylene	230	230	0.5	0.5
o-xylene	115	400	0.5	2
cyclopentane	4	7	0.7	1
n-hexane	5	7	0.6	1
n-octane	40	8	0.6	1
MTBE	230	--	0.5	--
PCE	80	--	1.2	--
TCE	101	--	1.4	--
1,1,2-TCA	695	--	1.4	--
cis-DCE	150	--	1	--
1,2-DCA	180	--	1	--

2.2. Analytical methods and data treatment

. The methods for concentration and for carbon and hydrogen isotope analysis are described in the Supplementary Material.

For all cases, isotope ratios are reported in the delta (δ) notation (Coplen, 2011):

$$\delta = \left(\frac{R}{R_{std}} - 1\right) \qquad \text{eq. 1}$$

where R and R_{std} are the isotope ratio of the sample and the international reference standard, respectively (VPDB for carbon and SMOW for hydrogen). The δ value obtained was then multiplied by 1000 to conveniently express it in units of per mil (‰).

For single step equilibrium conditions, the isotope fractionation caused by phase partitioning (between the gas and liquid) was quantified using:

$$\alpha = \frac{(1000+\delta_{gas})}{(1000+\delta_{liquid})} \quad \text{eq. 2}$$

Where α is the isotope fractionation factor, and where δ_{gas} and δ_{liquid} are the isotope values for the VOC in gas phase and in the liquid phase, respectively. For convenience, the isotope fractionation factor is further transformed into an isotope enrichment factor (ε) using:

$$\varepsilon = (\alpha - 1) * 1000 \quad \text{eq. 3}$$

An ANOVA test was carried out to evaluate difference between δ_{gas} and δ_{liquid} measurements, and the standard deviation reported for ε is the sum of the two standard deviations of the mean for each sample.

For multi stepwise equilibrium conditions, the general equation to quantify the isotope fractionation factor for NAPL-vapor equilibration and air-water partitioning was developed in Jeannottat and Hunkeler (2012):

$$\Delta\delta_{liquid} = \varepsilon(1 - f_{liquid}) \quad \text{eq. 4}$$

Where $\Delta\delta_{liquid}$ is the isotopic shift measured in the liquid, and f_{liquid} is the fraction of the VOC in the liquid. Since the latter expression was shown to provide equivalent results to the Rayleigh approach, the air-NAPL ($\varepsilon_{air\text{-}NAPL}$) and the air-water ($\varepsilon_{air\text{-}water}$) enrichment factor for each compound was quantified using the Rayleigh equation:

$$\ln\left[(\delta + 1000)/(\delta_i + 1000)\right] = \frac{\varepsilon}{1000}\ln f \quad \text{eq. 5}$$

Where δ_i is the initial isotopic composition of the compound, δ is the isotopic composition of the compound at the remaining fraction *f*.

For each compound, ε (for C and H) was determined by plotting $\ln\left[(\delta+1000)/(\delta_i+1000)\right]*1000$ as function of ln*f,* where ε is the slope of the linear regression. A slope was determined for each replicate and also by regrouping triplicate experiments as a whole to report the bulk slope. The slope was not forced through the origin, as suggested by Scott et al. (2004). A Student-T test for regression method (to validate a slope different than zero) and a 95% confidence interval (for slope uncertainty) were calculated using the Statistics module from Grapher-Golden software®.

Finally, the relationship Λ = H-$\varepsilon_{air\text{-}NAPL}$ / C-$\varepsilon_{air\text{-}NAPL}$ was applied to report Λvalues as H-$\varepsilon_{air\text{-}NAPL}$ and C-$\varepsilon_{air\text{-}NAPL}$ were determined in separate experiments. The Λ values contribute to enlarge the dataset used in the frame of 2D-CSIA approach to assess the dominant contaminant mass removal process during remediation treatment (Bouchard et al., 2018a).

2.3. Isotope modeling

A simple analytical simulation was performed describing the increasing VOC concentration into a solvent when an air stream loaded with gaseous VOCs is forced through. The analytical simulation incorporates isotope fractionation during dissolution process to investigate for potential isotope fractionation effect. The mathematical solution applied was previously described in Huybrechts et al. (2001):

$$C_L = \frac{C_g}{K}\left(1 - e^{\left(-\frac{KF}{V}\right)t}\right) \qquad \text{eq. 6}$$

Where C_L is the VOC concentration in the liquid at time *t*, C_g is the VOC concentration in the gas phase, *K* is the air-solvent partitioning constant for the VOC, *F* is the air flow rate passing through the solvent and *V* is the total volume of air injected. At infinite time (leading to VOC concentration equilibrium between gas and solvent), equation 6 simplifies to:

$$C_L = \frac{C_g}{K} \qquad \text{eq. 7}$$

To evaluate the isotope composition evolution of TCE used as the modeled compound, TCE molecules including a ^{13}C (^{13}C-TCE) or without (^{12}C-TCE) were distinguished (forming 2 isotopologues)

and modeled as two different contaminants. Different initial concentrations and air-solvent partitioning coefficients were attributed to each isotopologue, which were determinedas follow:

initial concentrations: For a given initial TCE concentration (C_{TCE}) in the gas stream and isotopic composition ($\delta^{13}C$), initial concentrations for ^{13}C-TCE ($C_{13C\text{-}TCE}$) and ^{12}C-TCE ($C_{12C\text{-}TCE}$) were determined using:

$$C_{13C-TCE} = \frac{C_{TCE}}{1+\frac{1000}{\delta^{13}C+1000}/R_{std}} \quad \text{eq. 8}$$

$$C_{12C-TCE} = \frac{C_{TCE}}{1+\frac{\delta^{13}C+1000}{1000}*R_{std}} \quad \text{eq. 9}$$

air-solvent partitioning constants: To account for isotope fractionation during dissolution, the air-TGDE isotope fractionation factor ($\alpha_{air\text{-}TGDE}$) for TCE determined in this study was used. The literature air-TGDE partitioning constant (*K*) was attributed to ^{12}C-TCE (K_L) and the *K* value for ^{13}C-TCE(K_H) was determined by:

$$\propto_{air-solvent} = \frac{K_H}{K_L} \quad \text{eq. 10}$$

The two isotopologues were independently treated to evaluate their respective accumulation in the solvent during a simulated sampling event. Forgiven periodicities, the simulated quantities of the two isotopologues were combined to calculate the $\delta^{13}C$. See Bouchard et al. (2011) for further explanation on the isotopic modeling approach.

Finally, a second simulation was performed to reproduce the isotope change measured during a multi step air-water equilibrium experiment. The equation 4 was expanded to include the number of equilibrium steps (*n*) as follow:

$$\Delta\delta^{n}_{liquid} = n\varepsilon(1 - f_{liquid}) \quad \text{eq. 11}$$

with

315 $$f_{liquid} = \left(\frac{C_n}{C_0}\right)^{1/n}$$ eq.12

316 where C_n and C_0 are respectively the concentration in aqueous phase after *n* equilibration steps and
317 Initial concentration in aqueous phase.

318

319 **3. Results**

320 **3.1. NAPL vaporization**

321 During stepwise NAPL vaporization of VOCs conducted in closed systems, the residual VOC mass
322 became progressively depleted in heavy carbon and hydrogen isotopes for all tested VOCs (Figure 1
323 and 2). The depletion trends indicate that molecules with heavy isotopes are more volatile than
324 those with light isotopes only. For carbon, the magnitude of isotope fractionation is small, but was
325 consistently reproduced over triplicate experiments. The carbon enrichment factors (C-$\varepsilon_{air\text{-}NAPL}$)
326 obtained for the bulk slope of the triplicates range between 0.14 ± 0.04 ‰ (cyclopentane) and 0.38 ±
327 0.05 ‰ (MTBE) (Table 2). The enrichment factors for aromatic compounds are within the same range
328 as aliphatic compounds, whereas the oxygenate compound (MTBE) provided a larger factor. For
329 hydrogen, the isotope enrichment factors (H-$\varepsilon_{air\text{-}NAPL}$) determined were at least an order of
330 magnitude larger than for carbon, and ranged between 2 ± 1‰ (MTBE) and 12 ± 2‰ (*n*-octane)
331 (Table 3). The hydrogen enrichment factors for aromatic compounds are smaller than for aliphatic
332 compounds, whereas the oxygenate compound (MTBE) provided a significantly smaller factor
333 compared to the two other groups. The variation of enrichment factors (C and H) among all tested
334 VOCs is best visualized when plotting H-$\varepsilon_{air\text{-}NAPL}$ values as function of C-$\varepsilon_{air\text{-}NAPL}$, where the resulting Λ
335 values (H-$\varepsilon_{air\text{-}NAPL}$ /C-$\varepsilon_{air\text{-}NAPL}$) allowed dissociating the 3 main compounds groups (Figure 3). The fuel
336 oxygenate (MTBE) provided the lowest Λ value (Λ=5), whereas the aliphatic compounds (*n*-octane,
337 cyclopentane and isooctane) provided the largest values (Λ ranging from 35 to 59), and with the
338 aromatic compounds (BT*o*-X) positioning in between (Λ ranging from 20 to 26).

339 **Table 2:** Carbon enrichment factors (C-$\varepsilon_{air\text{-}NAPL}$) related to stepwise NAPL vaporization and air-water
340 partitioning process in closed system experimental setups (measured in the current study) and
341 related to gas-phase diffusion and biodegradation (literature data) for selected aromatic, aliphatic,
342 oxygenate and chlorinated compounds.

Compound	Air-NAPL partitioning	Air-water partitioning	Gas-phase diffusion*	Aerobic biodegradation**
	ε (‰)			
Benzene	0.18 ± 0.03	n.s. to 0.09 ± 0.05	-1.71	-0.5 to-3.65
Toluene	0.22 ±0.04	n.s. to 0.17 ± 0.09	-1.28	n.d.to -3.3
Ethylbenzene	--	--	-1.00	-0.4 to -0.6[a]
m,p-Xylene	--	--	-1.00	-0.6 to-1.7 (*m*-X)
o-xylene	0.24 ± 0.04	n.s.	-1.00	--
n-octane	0.21 ± 0.03	--	-0.88	-0.7 to -1.1
cyclopentane	0.14 ± 0.04	--	-2.05	--
isooctane	0.17 ± 0.02	--	-0.88	--
MTBE	0.38 ± 0.05	0.22 ± 0.06	-1.42	-1.5 to-2.4
PCE	--	--	-0.45	--
TCE	--	--	-0.69	-11.6±4.1[b] to -18.2[c]
1,1,2-TCA	--	--	-0.66	--

343 n.s.= not significant. * calculated as described in Aelion et al. (2010), using 28,8 g/mol for air mass. **
344 In Aelion et al. (2010), if not specified. [a]Dorer et al. (2014), [b] Clingenpeel et al. (2012), [c] Barth et al.
345 (2002).

346

Table 3: Hydrogen enrichment factors (H-$\varepsilon_{air\text{-}NAPL}$) related to stepwise NAPL vaporization and air-water partitioning process in closed system experimental setups (measured in the current study) and related to gas-phase diffusion and biodegradation (literature data) for selected aromatic, aliphatic, oxygenate and chlorinated compounds.

Compound	Air-NAPL partitioning	Air-water partitioning	Gas-phase diffusion*	Aerobic biodegradation**
	ε (‰)			
Benzene	4 ± 1	-5 ± 1	-1.71	-11 to -17
Toluene	6 ± 1	-5 ± 2	-1.28	-8.6 to-159
Ethylbenzene	--	--	-1.00	+4 to -28[a]
m,p-Xylene	--	--	-1.00	--
o-xylene	6 ± 1	-9 ± 4	-1.00	--
n-octane	12 ± 2	--	-0.88	--
cyclopentane	9 ± 2	--	-2.05	--
isooctane	6 ± 1	--	-0.88	--
MTBE	2 ± 1	-9 ± 3	-1.42	-29 to -66
PCE	--	--	-0.45	--
TCE	--	--	-0.69	--
1,1,2-TCA	--	--	-0.66	--

* calculated as described in Aelion et al. (2010), using 28,8 g/mol for air mass. ** In Aelion et al. (2010), if not specified. [a]Dorer et al. (2014).

3.2. Air-water partitioning

During stepwise air-water partitioning of MTBE in closed systems, the remaining MTBE in the water became progressively depleted in heavy carbon isotopes, indicating that MTBE molecules with a heavy carbon isotope are more volatile than those including light carbon isotopes only (Figure 4). Significant change occurred for MTBE in both duplicate experiments, from which a carbon enrichment factor (C-$\varepsilon_{air\text{-}water}$) of 0.22 ± 0.06‰ was calculated based on the bulk slope of the two repetitions (Table 2). For benzene and toluene (with mass removed proportion $>$ 97%), only one repetition of each VOC showed a significant depletion trend (respectively C-$\varepsilon_{air\text{-}water}$ of 0.09 ± 0.05‰ and 0.17 ± 0.09‰), whereas the other two repetitions and the bulk slope of the three repetitions

indicated no significant change (Figure 4). Finally, no significant carbon isotope enrichment was observed for *o*-xylene in all three repetitions, for a mass removed proportion >97% (Figure 4). For hydrogen, in contrast, the residual VOC in water became progressively enriched in heavy hydrogen isotopes for every repetition of all four tested compounds (Figure 5), hence indicating that molecules with a heavy hydrogen isotope are less volatile than those with light hydrogen isotopes only. The bulk slope for BT*o*-X compounds respectively provided hydrogen enrichment factors (H-$\varepsilon_{air\text{-}water}$) of -5 ± 1‰, -5 ± 2‰ and -9 ± 4‰, whereas the oxygenate MTBE compound provided H-$\varepsilon_{air\text{-}water}$ = -9 ± 3‰ (Table 3).

3.3. Air-TGDE partitioning

Petroleum hydrocarbons: During single step air-TGDE partitioning in closed systems, the carbon isotope composition of gas phase aliphatic compounds (cyclopentane, *n*-hexane and *n*-octane) became enriched in heavy carbon isotopes, indicating that molecules with a heavy carbon isotope are less soluble in TGDE than molecules with light isotopes only (inverse isotope effect). The carbon enrichment factors (C-$\varepsilon_{air\text{-}TGDE}$) determined for the three aliphatic compounds tested were uniform and averaged 0.4 ± 0.2 ‰) (Table 4). For the aromatic compounds, in contrast, no significant isotopic change compared to the initial NAPL composition was measured for benzene, toluene, *m,p*-xylene and *o*-xylene (Table 4), with the exception of ethylbenzene. The isotopic composition of gas phase ethylbenzene became depleted in heavy carbon isotopes, indicating a normal isotope effect (C-$\varepsilon_{air\text{-}TGDE}$ = -0.6 ± 0.2‰). For hydrogen, the isotope composition measured for benzene and ethylbenzene in the gas-phase showed no significant change compared to the initial NAPL value, whereas the isotope composition of gas-phase toluene (H-$\varepsilon_{air\text{-}TGDE}$ = 6 ± 4 ‰) and *o*-xylene (H-$\varepsilon_{air\text{-}TGDE}$ = 28 ± 2 ‰) became enriched in heavy hydrogen isotopes (Table 4). Accordingly, molecules with a heavy hydrogen isotope are less soluble in TGDE than those with light isotopes only (inverse isotope effect). For the aliphatic compounds, no significant isotope composition change was observed for *n*-hexane

388 and *n*-octane, whereas the isotope composition of gas phase cyclopentane (H-$\varepsilon_{air\text{-}TGDE}$ = 6 $\pm$ 1 ‰)
389 became enriched in heavy hydrogen isotopes (Table 4).
390
391 *Chlorinated compounds:* gas-phase composition of all five chlorinated compounds tested (PCE, TCE,
392 1,1,2-TCA, *cis*-DCE and 1,2-DCA) became enriched in heavy carbon isotopes, indicating that molecules
393 with a heavy carbon isotope are less soluble in TGDE than molecules with light isotopes only (inverse
394 isotope effect) (Table 4). The C-$\varepsilon_{air\text{-}TGDE}$ determined for the chlorinated compounds ranged from 0.3 ±
395 0.2 ‰ (*cis*-DCE) to 1.1 ± 0.3 ‰ (1,1,2-TCA) (Table 4), which are generally larger than those
396 determined for petroleum hydrocarbons.
397

Table 4: C and H enrichment factors ($\varepsilon_{air\text{-}TGDE}$) related to air-TGDE partitioning process for selected aromatic, aliphatic, oxygenate and chlorinated compounds.

Compound	Carbon						Hydrogen				
	$\delta^{13}C$ (‰)				ε (‰)		$\delta^{2}H$ (‰)				ε (‰)
	pure	std	with TGDE	std	Thiswork	literature	pure	std	with TGDE	std	Thiswork
Benzene	-24.3	0.2	-24.1	0.1	*0.2 ± 0.2*	n.s.[a]	-52	1	-50	2	*2 ± 3*
Toluene	-26.4	0.2	-26.3	0.1	*0.1 ± 0.3*		-28	2	-22	2	6 ± 4
Ethylbenzene	-27.0	0.1	-27.6	0.1	-0.6 ± 02		-13	2	-9	2	*4 ± 4*
m,p-Xylene	-25.1	0.2	-25.2	0.1	*-0.1 ± 0.3*		-49	1	-47	1	*2 ± 2*
o-xylene	-29.2	0.1	-29.1	0.1	*0.1 ± 0.2*		-138	1	-114	1	24 ± 2
n-octane	-49.6	0.1	-49.3	0.1	0.3 ± 0.2		-213	3	-212	2	*1 ± 6*
n-hexane	-27.0	0.2	-26.6	0.1	0.4 ± 0.2		-101	2	-99	1	*2 ± 3*
cyclopentane	-22.6	0.1	-22.2	0.1	0.4 ± 0.2		-22	1	-16	1	6 ± 2
MTBE	-27.3	0.1	-27.7	0.1	0.4 ± 0.2		--	--	--	--	--
PCE	-26.5	0.1	-26.1	0.10	0.4 ± 0.2		--	--	--	--	--
TCE	-25.8	0.1	-24.8	0.1	1.0 ± 0.2	0.7 [a]	--	--	--	--	--
1,1,2-TCA	-33.6	0.2	-32.5	0.1	1.1 ± 0.3		--	--	--	--	--
cis-DCE	-22.9	0.1	-22.6	0.1	0.3 ± 0.2		--	--	--	--	--
1,2-DCA	-28.0	0.1	-27.1	0.1	0.9 ± 0.2		--	--	--	--	--

n.s.= not significant. [a]Bouchard et al. (2017b). Italic font indicates no significant change.

4. Discussion

4.1. Phase transfer isotope effect

The distribution of isotopologues between the gas phase and liquid phase upon equilibrium in closed systems is controlled by quantum mechanics, which accounts for the free energy involved for molecule translation, rotation and vibration in the system. The energy difference between the two isotopologues results in a vapor pressure isotope effect (VPIE) (Bigeleisen, 2006). The chemical environment provided by each phase will impact the energy distribution involved in the system. The chemical environment in the gas phase is governed by the intramolecular (vibrational) forces, while the chemical environment in the liquid phase is governed by the intermolecular forces (rotation and translation) and the intramolecular forces (Bigeleisen, 2006). Therefore, the different chemical environment provided by the NAPL compared to water is expected to influence the direction (inverse

413 or normal isotope effect) and the magnitude of the isotope fractionation. For partitioning systems
414 where the solute is dissolved into water, the isotope effect related to a different solubility property
415 (i.e. the Henry constant) of each isotopologue can be evaluated using the same theoretical
416 considerations (i.e. translation, rotation and vibration energy) as for the NAPL system described
417 above (Jancso, 2002).The discussion below will first treat results involving NAPL vaporization, and will
418 be followed by results obtained when VOC is a solute in water.

419

420 **4.1.1. Isotope fractionation during stepwise NAPL vaporization**

421 The results of all experiments evaluating NAPL vaporization for a selection of petroleum
422 hydrocarbons and one fuel oxygenate consistently underlined a higher volatility for molecules with a
423 heavy isotope (either a ^{13}C or ^{2}H), hence producing an inverse isotope fractionation effect. This
424 inverse direction of the isotope fractionation observed for hydrocarbons was expected as previously
425 discussed by Van Hook (2006) and reflects the interaction of intramolecular and intermolecular
426 molecular forces in the NAPL. An inverse isotope effect is generated when the effect of
427 intramolecular forces associated with vaporization becomes larger than the effect of intermolecular
428 forces in the NAPL. For hydrocarbons, the reduction of the vibrational frequencies of molecules in
429 the NAPL relatively to the air-phase due to interactions among the molecules creates this inverse
430 isotope effect (Jancso and Van Hook, 1974). The reduced vibrational frequencies for hydrocarbons
431 was empirically rationalized by Bartell and Roskos (1966)to be caused by longer C–H bonds compared
432 to C–D bonds, which leads to a preferential retention of light isotopes in the NAPL. However, this
433 empirical molar vapor isotope effect (MVIE) does not consider the temperature effect, and only
434 applies to liquids near the melting point (Van Hook, 2006). Furthermore, theoretical calculations
435 performed by Lacks (1995) underlined the necessity to consider additional intermolecular effects
436 (intermolecular separations) to more accurately foresee MVIE.

437 The magnitude of $\varepsilon_{air\text{-}NAPL}$ values determined in this study compare well to the very few values
438 available in the literature determined using similar closed system experimental setups. For carbon,
439 similar depletion magnitudes of heavy isotopes in the NAPL caused by vaporization were observed
440 for benzene and for toluene (Table S-1 in Supplementary Material). For hydrogen, larger H-$\varepsilon_{air\text{-}NAPL}$
441 were expected compared to carbon as the isotope effects in general depend on the masses of the
442 isotopic atoms involved and the force constants bonding 2 atoms in the molecule (Van Hook, 2006).
443 The H-$\varepsilon_{air\text{-}NAPL}$ determined for benzene and toluene in this current study are also in good agreement
444 with older literature (Table S-2 in Supplementary Material). It should be noted that studies
445 conducted with open system experimental setups (i.e. non-equilibrium conditions such as
446 progressive NAPL vaporization from an open beaker in a fume hood) give enrichment factors that
447 cannot be compared to our values due to additional isotope effects brought by diffusion (Kuder et
448 al., 2009; Jeannottat and Hunkeler, 2012; Julien et al., 2015a). The impact of open system
449 experimental setups on isotope fractionation is discussed further in section 4.1.3. Table S-1 and S-2 in
450 Supplementary Material summarize $\varepsilon_{air\text{-}NAPL}$ values determined for C and H, respectively, for studies
451 conducted using open system experimental setups.

452 The results of the current study for closed systems revealed smaller carbon isotope fractionation for
453 petroleum hydrocarbons (carbon atoms number ranging from 5 to 8) compared to fuel oxygenate (5
454 carbon atoms) (Table 2) and also compared to chlorinated compounds (2 carbon atoms) (Table S-1).
455 It must be considered that the C-$\varepsilon_{air\text{-}NAPL}$ values reported are “bulk” isotope effect, contrasting with
456 the concept of specific reactive position as considered for kinetic isotope fractionation during
457 biodegradation (Elsner et al., 2005). For thermodynamic isotope fractionation at equilibrium
458 conditions, the molecular structure and the positioning of the heavy isotope were shown to be of
459 importance (Van Hook, 2006). While all positions are considered reactive, the positioning of the
460 heavy isotope at the terminal position of a molecule is expected to lead to larger isotope
461 fractionation (Bigeleisen and Ishida, 1973). This terminal-position specific impact for carbon was
462 addressed for heptane by Julien et al. (2015a), but the difference in isotope fractionation compared

463 to the other position was very small. The latter study additionally showed minor position-specific
464 isotope fractionation for toluene. For hydrogen, isotope fractionation of monodeuterated benzene
465 (C_6H_5D) was shown to be equivalent to 1/6 of the isotope fractionation of perdeuterated benzene
466 (C_6D_6) (Jakli et al., 1978), thus also suggesting no significant reactive position for hydrogen as well for
467 petroleum hydrocarbons. Our results agree with this lack of reactive-position isotope fractionation,
468 showing no clear trend between isotope enrichment factors obtained for petroleum hydrocarbons
469 and increasing number of C or H atoms (Table 2). Therefore, the larger C-$\varepsilon_{air\text{-}NAPL}$ values for MTBE and
470 TCE are more likely related to the presence of the oxygen or chlorine atoms in the molecule,
471 respectively, impacting more significantly the vibrational frequencies of molecules in the NAPL phase
472 compared to petroleum hydrocarbons. Furthermore, the molecular structure and H-saturation
473 extent of petroleum hydrocarbon seems to be a distinctive aspect for H-$\varepsilon_{air\text{-}NAPL}$ values, as discernible
474 on Figure 3 where Λ values distinguish the aromatic compounds from aliphatic and fuel oxygenate
475 compounds. Distinction is mainly due to the various magnitudes of H-$\varepsilon_{air\text{-}NAPL}$ values. While the
476 molecular structure impacts differently the motion (rotation and translation) of molecules in the
477 NAPL phase, hydrogen bonds and different polarization potential of molecules also contribute to the
478 isotope fractionation (Lacks, 1995; Wade, 1999). In our case, the electrical configuration of aliphatic
479 compounds (involving H-saturation) suggests a stronger polarization impact on the H-$\varepsilon_{air\text{-}NAPL}$ values
480 compared to aromatic rings (involving π electrons) and MTBE. This polarization impact trend on the
481 H-$\varepsilon_{air\text{-}NAPL}$ values for the three different groups respect the polarizability potential expressed by each
482 group, with aliphatics having the least polarizability potential and MTBE having the largest (Reichardt
483 and Welton, 2010). However, this polarizability potential impact trend is not respected when
484 considering chlorinated solvents. A H-$\varepsilon_{air\text{-}NAPL}$ value for TCE larger than for petroleum hydrocarbons
485 was reported in the literature (Table S-2) while the polarizability potential would predict a smaller
486 value, hence suggesting additional chemical interactions contributing to isotope fractionation for
487 chlorinated solvents.

488

4.1.2. Isotope fractionation caused by stepwise air-water partitioning

The air-water partitioning experiments conducted in this study indicated that the partitioning of BTo-X compounds between the air and water (polar protic solvent) does not create significant carbon isotope fractionation (not significant in 2 out of 3experiments). Our results for toluene agree with the published work investigating this process using a closed system experimental setup (Table S-1). This absence of a systematic carbon isotope fractionation for BTo-X is contrasting with the systematic, yet small, observed carbon isotope fractionation caused by NAPL vaporization (Table 2). While for MTBE the air-water partitioning process created a significant inverse carbon isotope fractionation (C-$\varepsilon_{air\text{-}water}$ = 0.22$\pm$0.06 ‰), the latter process also created a smaller isotope fractionation compared to air-NAPL vaporization (C-$\varepsilon_{air\text{-}NAPL}$ = 0.38 $\pm$0.05 ‰), which is in agreement with MTBE values reported by previous works using similar experimental setups (Table S-1). Based on different isotope fractionation magnitude obtained for the two liquids, the intermolecular forces applied by the water on aromatic compounds and MBTE seem to generate a smaller difference in free energy between heavy and light isotopes than the NAPL phase, which is leading to smaller isotope fractionation. This trend for larger carbon isotope fractionation caused by air-NAPL vaporization compared to air-water partitioning was also observed for TCE by Jeannottat and Hunkeler (2012) and Horst and Lacrampe-Couloume (2020) (Table S-1). The reported C-$\varepsilon_{air\text{-}water}$ values for TCE are larger compared to BT*o*-X and MTBE determined herein. In this case, the presence of chlorine atoms in the molecules and the different molecular structure of chlorinated compounds compared to aromatic compounds are likely impacting differently the intermolecular forces with water. As mentioned above, values derived from open system experimental setups cannot be compared to our values but are summarized in Table S1 and S-2 respectively for carbon and hydrogen.

For hydrogen, the normal isotope fractionation observed during air-water partitioning is contrasting with the inverse hydrogen isotope fractionation observed for air-NAPL vaporization, as predicted when changing the chemical environment from a nonpolar to a hydrogen bonded liquid (Wolfsberg et al., 2010). In this case, the motion forces (rotation and translation) exerted by water molecules

surrounding BTX and MTBE compounds outweigh the vibrational forces, generating higher volatility for molecules including a heavy hydrogen isotope in the molecular structure. The motion forces seem more impactful for *o*-xylene and MTBE compared to benzene and toluene, generating a smaller H-$\varepsilon_{air\text{-}water}$ value for the latter two compounds (Table 3). For MBTE, the polar nature of the compound likely initiating stronger interactions with water molecules would explain the larger H-$\varepsilon_{air\text{-}water}$ value compared to benzene and toluene. However, the forces leading to larger H-$\varepsilon_{air\text{-}water}$ value for *o*-xylene compared to benzene and toluene requires more detailed investigations. In addition, the normal isotope fractionation for TCE (H-$\varepsilon_{air\text{-}water}$= 5.2 $\pm$2.6 ‰) and for trichloromethane recently reported by Horst and Lacrampe-Couloume (2020) and contrasting with the inverse isotope fractionation obtained herein for aromatic compounds and MTBE would also require more detailed investigations.

4.1.3. Significance for gas-phase VOC assessments

Extending the application of CSIA to soil gas studies will significantly improve assessment strategies relying on VOC concentration measurements such as NSZD monitoring or remediation treatments like SVE or air-sparging systems. The enrichment factors determined in this study during volatilization of common subsurface contaminants contributes to increase the number of VOC candidates for CSIA-based assessments. However, ε values for CSIA data interpretation should be cautiously selected. Whilst our study focused on closed system experiment setups (i.e. equilibrium conditions) to determine isotope fractionation strictly related with the phase partitioning process, several other studies have reported values determined using open system experiment setups (i.e. non-equilibrium conditions). In the latter case, the gas-phase volume above the liquid is constantly renewed at an experiment-specific rate, hence involving additional physical isotope fractionation process such as gas-phase diffusion. Table S-1 and S-2 (in Supplementary Material) compiles respectively carbon and hydrogen isotope fractionation factors determined using open system experiment setups for VOC volatilization from NAPL or water. One can note a wider ε value range for open system experimental setups, even observing opposite fractionation direction in the case for carbon, thus confirming the contribution of one or several other isotope fractionation processes. For a porous system with very

541 slow air renewal rate, one can assume quasi-equilibrium conditions to control the isotope
542 fractionation evolution in the soil air immediately surrounding the residual NAPL. In contrast, non-
543 equilibrium conditions would control the isotope fractionation evolution during forced air flow
544 circulation applied by specific remediation treatment systems. Therefore, the interplay of physical
545 processes (i.e. phase transfer and diffusion) must be properly considered to correctly interpret CSIA
546 field data. For instance, during NSZD of trapped NAPL in the unsaturated zone, NAPL vaporization
547 leads to VOC mass input into soil gas and pore water. With small C-$\varepsilon_{air\text{-}NAPL}$ and insignificant C-$\varepsilon_{air\text{-}water}$
548 determined for BTX, progressive NAPL vaporization will not create significant change in isotope
549 composition of gas-phase VOCs over time as long as the gas-phase VOC concentration in soil air
550 remains in equilibrium with the NAPL (i.e. steady state condition) (Bouchard et al., 2008a; Bouchard
551 et al., 2011). This can also be assumed although the occurrence of biodegradation as the kinetic rate
552 of VOC mass input at the NAPL fringe may overwhelm the biodegradation rate, hence masking the
553 isotopic effect of the latter as commonly observed for groundwater assessments within source zone
554 areas. However, once the VOC mass in the NAPL has significantly decreased and equilibrium
555 conditions can no longer be maintained, hence initiating a transient state condition, gas-phase
556 diffusion process will lead isotope composition towards enriched values. For all petroleum
557 hydrocarbons tested herein, the larger carbon isotope fractionation related to gas-phase diffusion
558 (Table 2) will dominate over air-NAPL partitioning. This evolution from constant to gradually enriched
559 isotope composition appears to be a more reliable metric than concentration analysis to support
560 source vanishing. Given the small and narrow range of C-$\varepsilon_{air\text{-}NAPL}$ values determined for petroleum
561 hydrocarbons herein, similar enrichment trends can be expected for other petroleum hydrocarbons
562 such as ethylbenzene and trimethylbenzene, hence allowing additional compounds to be assessed.
563 For hydrogen, with inverse H-$\varepsilon_{air\text{-}NAPL}$ and normal H-$\varepsilon_{air\text{-}water}$ values determined for BTX (Table 3), the
564 interplay between air-NAPL, air-water and gas-phase diffusion during steady and transient state
565 conditions should be further investigated to confidently predict the direction and the magnitude of
566 the isotope change.

For remediation techniques focusing on physical mass removal process such as SVE systems, the air-liquid isotope effects can be exploited to monitor the progress and the limitations of the treatment. Contrasting with NSZD, the isotope composition in this case will evolve as for an open system (i.e. non-equilibrium conditions). During non-equilibrium conditions, not only that the diffusive isotope effect is additive to air-liquid isotope effect, but a number of studies have previously described that the expression of the diffusive isotope effect is impacted by the air volume renewal rate (Bouchard et al., 2008a; Bouchard et al., 2008b; Höhener et al., 2008; Kuder et al., 2009; Julien et al., 2015b; Bouchard et al., 2017a; Zamane et al., 2020). In cases where biodegradation occurs during the VOC transit through the unsaturated soil (as for petroleum hydrocarbons), this third process will also need to be considered to appropriately interpret isotopic trends. Due to those many uncertainties, the mass removal process is best characterized with the use of two elements (i.e. dual-isotope assessment) (Kuder et al., 2009; Bouchard et al., 2017a). To appreciate the additive isotope effects on VOCs studied herein, enrichment factors related to gas-phase diffusion and biodegradation under aerobic conditions are reported in Table 2 and 3, respectively for carbon and hydrogen. For carbon, the diffusion effect will systematically mask both the air-NAPL and air-water partitioning effects for every petroleum hydrocarbon tested, leading to carbon isotope enrichment (as biodegradation does). For hydrogen in contrast, the air-NAPL partitioning is the only process leading to significant hydrogen isotope depletion. Thorough combined interpretation of the carbon and hydrogen isotope evolution pattern over time will therefore indicate the controlling mass-removal process.

4.2. TGDE and isotope fractionation

4.2.1. Isotope fractionationcaused by air-TGDE partitioning

Despite a single equilibration step, C-$\varepsilon_{air\text{-}TGDE}$ values determined for air-TGDE partitioning (Table 4) can be directly compared to ε values derived by multistep equilibration experiments based on equation 4.Accordingly, the lack of significant carbon isotope fractionation observed for benzene, toluene and both xylenes during air-TGDE partitioning is akin to inconsistent carbon isotope fractionation observed for the same compounds during air-water partitioning and also to the lack of significant

593 carbon isotope fractionation previously reported for benzene during similar testing with TGDE
594 (Bouchard et al., 2017b). These non-significant carbon isotope fractionations observed for BTX
595 compounds during air-TGDE partitioning underline minor impact for phase transfer process, and
596 where the prevailing partitioning forces would be more comparable to water than neat compounds.
597 The significant fractionation obtained for ethylbenzene, in contradiction to the other 4 aromatic
598 compounds tested, are counter intuitive. Additional evaluations are needed to understand this
599 distinctive behavior. In contrast to aromatic compounds, the phase transfer process involving
600 aliphatic and chlorinated compounds generated significant isotope fractionation. The global set of
601 chlorinated compounds showed isotope fractionation generally of larger magnitude, with chlorinated
602 ethane compounds more likely to generate larger fractionation compared to chlorinated ethene
603 compounds (Table 4). The lack of available works assessing isotope fractionation of aliphatic and
604 chlorinated compounds during air-water and air-NAPL partitioning, however, limits the comparison
605 with air-TGDE. For PCE, the C-$\varepsilon_{air\text{-}TGDE}$ value determined (0.4 $\pm$ 0.2 ‰) is in the range of the C-$\varepsilon_{air\text{-}water}$
606 value reported by Jeannottat and Hunkeler (2013) (0.46 $\pm$ 0.04 ‰), although no air-NAPL partitioning
607 values for PCE are available for comparison. For TCE, the C-$\varepsilon_{air\text{-}TGDE}$ values determined (1.0 $\pm$ 0.2 ‰)
608 and previously reported (0.7 ‰) (Bouchard et al., 2017b) are in the range of reported C-$\varepsilon_{air\text{-}NAPL}$ values
609 (ranging from 0.4 to 1.0 ‰), and slightly larger than the reported C-$\varepsilon_{air\text{-}water}$ range values (0.4 to 0.7
610 ‰) (Table S-1 in Supplementary Material). The result comparison for different compounds outlines
611 some partitioning specificities. Overall, this polar aprotic solvent with multiple ether oxygen atom
612 functional groups generates inverse carbon isotope effect as for water and NAPL, with magnitude of
613 isotope fractionation being larger for chlorinated compounds compared to aromatic and aliphatic
614 compounds. Once more, the degree of H saturation of the molecules and the presence of chlorine
615 atoms in chlorinated compounds seem to be responsible for the various isotope fractionation
616 magnitudes observed for those three different types of compounds.
617

For hydrogen, no clear molecular structural trend can be outlined when comparing compounds expressing no isotope fractionation (benzene, ethylbenzene, *m,p*-xylene, *n*-hexane and *n*-octane) with those undergoing isotope fractionation (toluene, *o*-xylene and cyclopentane) during air-TGDE partitioning. Nonetheless, the inverse isotope fractionation observed for aromatic and aliphatic compounds during air-TGDE partitioning, when significant, is analogous to air-NAPL vaporization, and is contrasting with the normal isotope fractionation observed for air-water partitioning. The magnitude of H-$\varepsilon_{air\text{-}TGDE}$ values determined for toluene and cyclopentane are relatively in the same range or lower than for NAPL vaporization, hence suggesting that the vibrational forces out weighting the motion forces in TGDE are similar to the air-NAPL system, and that functional groups of TGDE act on those compounds differently than do water molecules. In this regard, influence of different functional groups causing isotope fractionation was recently investigated using benzene and toluene as tested compounds (Imfeld et al., 2014). The latter study demonstrated the occurrence of isotope fractionation for specific functional groups represented by a subset of different organic solvents. For instance, 1-octanol (hydroxyl functional group with hydrogen-bridging interaction) led to significant inverse carbon and hydrogen isotope fractionation for benzene. However, as their experimental setup involved solute partitioning into two liquids (solvent and water), the additional hydrophobic factor impacting the isotope fractionation impedes direct ε comparison with our study. Finally, the larger H-$\varepsilon_{air\text{-}TGDE}$ value determined for *o*-xylene compared to the other aromatic compounds is prominent. Additional evaluations are needed to understand this distinctive behavior.

4.2.2. TGDE and gas-phase VOC sampling

Gas-phase sampling process: an innovative solvent-based method has been recently developed to perform CSIA on VOCs collected in the gas-phase (Bouchard et al., 2015). The sampling method consists in pulling the ambient air through a solvent via an adapted sampling device, hence relying on the VOC affinity with the solvent to accumulate (by dissolution) during the sampling process. To evaluate TCE dissolution efficiency and the potential for isotope fractionation during the process, a

gas-phase sampling event was mimicked at the laboratory scale (see Bouchard et al. (2017b) for further experimental details). While the measured dissolved TCE concentrations in TGDE over time followed the theoretical expectation (equation 6), no $\delta^{13}C$ evolution simulation was attempted to reproduce the measured isotope values. The equation 6 and C-$\varepsilon_{air\text{-}TGDE}$ were used herein to scrutinize the potential carbon isotope fractionation caused during the sampling process and to reproduce the isotope values measured over the 3 mimicked gas-phase sampling events. The calculations made use of two TCE isotopologues (^{13}C-TCE and ^{12}C-TCE) as described in section 2.4. Both C-$\varepsilon_{air\text{-}TGDE}$ values available (0.7 ‰ and 1.0 ‰) were sequentially implemented to evaluate the sensitivity of the parameter. Table 5 summarizes the values used for ^{13}C-TCE and ^{12}C-TCE isotopologues for the calculations, as well as the fixed parameters.

Table 5: Initial gas phase concentration (Cg) and air-TGDE partitioning coefficient (*K*) specific to ^{13}C-TCE and ^{12}C-TCE isotopologues, TCE initial isotopic composition ($\delta^{13}C$), air flow rate (*F*) and volume of solvent (*V*) used for the analytical simulation.

	Simulation 1		**Simulation 2**		**Simulation 3**	
Parameter	**^{12}C-TCE**	**^{13}C-TCE**	**^{12}C-TCE**	**^{13}C-TCE**	**^{12}C-TCE**	**^{13}C-TCE**
Cg (ug/m3)	20.7736	0.2264	78.1484	0.8516	165.1999	1.8001
K (unitless) with $\varepsilon_{air\text{-}TGDE}$= 0.7‰	0.0003400[a]	0.0003402	0.0003400[a]	0.0003402	0.0003400[a]	0.0003402
K (unitless) with $\varepsilon_{air\text{-}TGDE}$ =1.0‰	0.0003400[a]	0.0003403	0.0003400[a]	0.0003403	0.0003400[a]	0.0003403
F (mL/minute)	800		200		100	
V (mL)	35		35		35	
Initial $\delta^{13}C$ (‰)	-30.3		-30.3		-30.3	

a(Bouchard et al., 2017b)

The simulated dissolved concentration and $\delta^{13}C$ results obtained for three different gas-phase TCE concentrations (21, 79 and 167 µg/m^3) over a sampling duration of t = 50h are presented on Figure 6. The simulated concentrations indicate a non-linear TCE increase in TGDE during the sampling process. The steady state is reached (i.e. saturation condition) within 10h for the smallest gas-phase concentration (figure 6a, 21 µg/m^3), while a quasi-steady state is reached around t = 50h for gas-phase concentration of 79 µg/m^3 (figure 6b), and a transient state is still observed at t=50h for the gas-phase concentration of 167 µg/m^3 (Figure 6c). Note that the difference in concentration evolution is due to different sampling flow rates used (Table 5), and not the gas-phase concentration.

During the sampling event, the isotopic composition of dissolved TCE evolved from -30.30 ‰ (equivalent to the gas-phase TCE composition) to a maximum depleted value of -30.98 ‰ (using C-$\varepsilon_{air\text{-}TGDE}$ = 0.7 ‰) and -31.25 ‰ (using C-$\varepsilon_{air\text{-}TGDE}$ = 1.0 ‰) when saturation conditions are reached (Figure 6A). At early sampling phase, the higher solubility of ^{12}C-TCE is not yet apparent, hence the dissolved TCE isotope composition was reflecting the gaseous TCE isotope composition. With time, the higher solubility of ^{12}C-TCE eventually disrupts the initial ^{13}C-TCE / ^{12}C-TCE mass proportion, which leads to a gradual depleting isotope trend. The shift of 0.68 ‰ and 0.95 ‰ observed at saturation conditions compared to the source signal (Figure 6A) is respectively equivalent to the C-$\varepsilon_{air\text{-}TGDE}$ of 0.7‰ and 1.0 ‰ experimentally determined (Table 4). Moreover, this slight isotopic depletion trend provided by the analytical solution was able to reproduce the measured laboratory values, validating the impact of different solubility coefficient for the two distinct TCE isotopologues. While laboratory results for gas-phase TCE at 21 µg/m^3 (Figure 6A) and 167 µg/m^3 (Figure 6C) are mostly contained within the variation expressed by the two different C-$\varepsilon_{air\text{-}TGDE}$ values, the laboratory results for gas-phase TCE at 79 µg/m^3 (Figure 6B) showed good fit only at later time (quasi-steady state). This can perhaps be related to a gas leak in the system delivering less TCE than expected.

According to these isotopic simulations, sampling gas phase VOCs using TGDE (or any other solvent) will create an isotopic shift that can be predicted by the $\varepsilon_{air\text{-}TGDE}$ value. Based on $\varepsilon_{air\text{-}TGDE}$ values reported in Table 4 for the tested VOCs, no significant carbon isotope shift is expected for BTX, aliphatic compounds (*n*-octane, *n*-hexane, cyclopentane), MTBE, PCE and *cis*-DCE, no significant hydrogen isotope shift is expected for B, E, *m,p*-X, *n*-hexane and *n*-octane, and lastly no significant chlorine isotopic shift for TCE, as respective $\varepsilon_{air\text{-}TGDE}$ value is either not detectable or within the common analytical uncertainty of 0.5 ‰ (for C and Cl) and 5 ‰ (for H). However, carbon isotope measurements for ethylbenzene, TCE, 1,1,2-TCA and 1,2-DCA, and hydrogen isotope measurement for toluene, *o*-xylene and cyclopentane will request an adjustment for sampling conducted until the

691 saturation condition is reached. In this case, the equivalence of the $\varepsilon_{air\text{-}TGDE}$ value has to be added to
692 provide a more positive final $\delta^{13}C$ composition (or more negative in the case of ethylbenzene).

693 *Post sampling event:* An additional simulation was further carried out to evaluate the impact of
694 repeated headspace volume exchange potentially occurring during sample handling and storage on
695 the isotope composition of the dissolved VOCs. This evaluation made use of equation 11 to calculate
696 the related hydrogen isotopic shift caused by multi equilibrium steps using either TGDE or water as
697 solvent. Between each equilibrium step, a complete headspace renewal with fresh air was
698 considered. For the evaluation purpose, toluene was the modeled compounds as results of the air-
699 water and air-TGDE partitioning experiments performed in the laboratory led to significant hydrogen
700 isotope fractionation. In addition, the dataset collected during the air-water partitioning experiment
701 can be used as reference to validate the calculations. Table 6 summarizes the parameters and
702 coefficients used for those two air-liquid partitioning evaluations.

703 **Table 6:** Parameters used to calculate the hydrogen isotope shift expected for toluene caused by
704 multistep air-water or air-TGDE partitioning process (equilibrium conditions).

Parameter	Coefficient	Unit
H-$\varepsilon_{air\text{-}TGDE}$	6*	‰
H-$\varepsilon_{air\text{-}water}$	-5**	‰
C_0	1	µg/L
Air-water partitioning (Henry coefficient, at 25 °C)	0.244[a]	unitless
Air-TGDE partitioning (*K*, at 25 °C)	0.000344[b]	unitless
Vial volume	40	mL
Liquid volume	35	mL

705 *This study. ** Value obtained for replicate 2, Figure 5. [a]Mackay et al. (2006). [b]Huybrechts et al. (2001)

706 Changes in hydrogen isotope composition of dissolved toluene caused by 12 equilibrium steps with
707 water or TGDE are shown on Figure 7. For the air-water partitioning simulation, the equation
708 reproduced well the isotopic trend observed with the laboratory experiment, to ultimately predict a
709 significant hydrogen shift of 11.8 ‰ after 12 equilibration steps. For the air-TGDE partitioning
710 simulation, a shift of 0.03 ‰ can be expected for the hydrogen isotope composition of dissolved
711 toluene dissolved after proceeding to 12 equilibration steps. Compared to a common uncertainty

712 error of 5 ‰ for hydrogen analysis, this shift remains not significant. This negligible isotopic impact is
713 explained by the strong affinity of toluene with TGDE, providing a very small air-TGDE partitioning
714 coefficient (Table 6). Upon equilibrium, a mass fraction of 99.97% of toluene is expected to be in
715 TGDE, thus leaving a small 0.03% mass fraction in the gas-phase. This very small mass fraction of
716 gaseous toluene lost by each equilibrium step is not sufficient to significantly impact the isotope
717 signature of toluene dissolved in TGDE, although several multiple equilibrium steps are carried out.
718 This is in agreement with Bouchard et al. (2015) reporting no significant change in the carbon isotope
719 composition of TCE after 12 months of storage in methanol. Therefore, although carbon and
720 hydrogen isotope fractionation have been observed for diverse VOCs during the air-TGDE
721 partitioning process, no further impacts on the isotopic signature of dissolved VOCs is expected once
722 the sampling process is ended. This can be assumed for every compound with similar low range of
723 air-TGDE partitioning coefficients than toluene.
724
725 **5. Conclusion**
726 Several types of laboratory experiments were conducted in the present study to evaluate isotope
727 fractionation caused by phase transfer process for a selection of common environmental
728 contaminants, with the general objective being to contribute in expanding the use of CSIA as an
729 assessment tool for gas-phase studies. For this purpose, the occurrence of isotope fractionation
730 related to NAPL vaporization and VOC volatilization from different liquids (water or TGDE) was
731 investigated through closed system experimental setups. In contrast to open system, conducting
732 stepwise VOC mass removal from a closed system setup insures the isolation of the partitioning
733 process from other potential physical process. A selection of aromatic, aliphatic, fuel oxygenate and
734 chlorinated compounds was evaluated for carbon and hydrogen isotope fractionation. NAPL
735 vaporization consistently indicated a preferential volatility for molecules including a heavy isotope,
736 either ^{13}C or ^{2}H isotope, for all tested VOCs. The magnitude of the carbon isotope enrichment was
737 small and relatively uniform among the selected petroleum hydrocarbons, and globally smaller
738 compared to chlorinated compounds. The magnitude of the hydrogen isotope enrichment was more

739 substantial and distinctive among petroleum hydrocarbons, but still globally smaller compared to
740 chlorinated compounds. The carbon and hydrogen isotope fractionation pattern, evaluated through
741 the Λ value, was found to differ between aromatic, aliphatic and fuel oxygenate compounds.
742 Furthermore, during VOC volatilization from the water, the partitioning process led to no significant
743 carbon isotope fractionation for aromatic compounds. These observations for aromatic compounds
744 contrast with significant fractionation observed for MTBE and the reported isotope fractionation for
745 chlorinated compounds (PCE and TCE), underlying for the latter three compounds a higher volatility
746 for molecules including a heavy carbon isotope. In contrast, for hydrogen, volatilization of BTX
747 compounds from water consistently created a normal isotope fractionation, translating into a
748 preferential solubility for molecules including the heavy hydrogen isotope. The numerous isotope
749 enrichment factors derived in this study relative to NAPL vaporization and air-water partitioning
750 process provide the possibility to expand the application of CSIA to a broader range of common
751 environmental contaminants in view to assess their fate in the unsaturated zone, either passively
752 attenuating (for instance, to document a natural source zone depletion in the unsaturated zone) or
753 actively removed (for instance, to assess the performance of a remediation treatment). The second
754 goal of this study was also achieved by quantifying carbon and hydrogen isotope enrichment factors
755 related to air-TGDE partitioning for a subset of VOCs. For carbon, most of the aromatic compounds
756 tested led to no significant isotope fractionation (except ethylbenzene), whereas MTBE, aliphatic and
757 chlorinated compounds led to significant enrichment, underlying potential for higher volatility of
758 molecules including a heavy isotope similarly to progressive NAPL vaporization. The carbon isotope
759 composition of chlorinated compounds was found to be more affected than petroleum hydrocarbons
760 by air-TGDE partitioning. For hydrogen, selected aromatic and aliphatic compounds showed no
761 significant enrichment, except for toluene, *o*-xylene and cyclopentane, which showed significant
762 enrichment. When significant, both isotopes underlined the potential for higher volatility of
763 molecules including a heavy isotope similarly to progressive NAPL vaporization. The impact of isotope
764 fractionation related to air-TGDE partitioning during a sampling event using TGDE as a sink matrix to

765 collect gas-phase VOCs was further addressed by means of analytical simulations. The simulation
766 results indicated an isotopic shift equivalent to the enrichment factors, once the VOC concentration
767 equilibrium between the air and TGDE is reached. Therefore, the need for an isotopic correction post
768 sampling event only applies to VOCs having an enrichment factor larger than the GC-IRMS analytical
769 uncertainty. The quantification of enrichment factors by the current investigations and the
770 knowledge gained through analytical simulations support the field application of the solvent-based
771 sampling method specific to CSIA. Although a broad range of common environmental contaminants
772 were evaluated for carbon and hydrogen isotopes, potential for chlorine isotope fractionation
773 remains to be evaluated for chlorinated compounds.

774 **Supplementary Material: Description of analytical techniques, Tables S1+S2,**

775 **Is available.**

776 **Acknowledgments**

777 The authors are grateful to the former Chevron Energy Technology Company (now Chevron Technical
778 Center) for the financial support needed to conduct laboratory experiments related to the air-NAPL
779 and air-water partitioning investigation.

780 **References**

781 Aelion, C.M., Höhener, P., Hunkeler, D., Aravena, R. (Eds.), 2010. Environmental isotopes in
782 biodegradation and bioremediation. CRC Press. Taylor and Francis Group, Boca Raton, London, New
783 York.
784 Baker, R.J., Baehr, A.L., Lahvis, M.A., 2000. Estimation of hydrocarbon biodegradation rates in
785 gasoline-contaminated sediment from measured respiration rates. Journal of Contaminant Hydrology
786 41, 175-192.
787 Bartell, L.S., Roskos, R.R., 1966. Isotope Effects on Molar Volume and Surface Tension: Simple
788 Theoretical Model and Experimental Data for Hydrocarbons. The Journal of Chemical Physics 44, 457-
789 463.
790 Barth, J.A., Slater, G., Schüth, C., Bill, M., Downey, A., Larkin, M., Kalin, R.M., 2002. Carbon isotope
791 fractionation during aerobic biodegradation of trichloroethene by Burkholderia cepacia G4: a tool to
792 map degradation mechanisms. Appl Environ Microbiol 68, 1728-1734.
793 Beckley, L., McHugh, T., Philp, P., 2016. Utility of Compound-Specific Isotope Analysis for Vapor
794 Intrusion Investigations. Groundwater Monitoring & Remediation 36, 31-40.
795 Bigeleisen, J., 2006. Theoretical Basis of Isotope Effects from an Autobiographical Prespective. in:
796 Kohen, A., Limbach, H.-H. (Eds.). Isotope Effects in Chemistry and Biology. Taylor & Francis Group,
797 Boca Raton, p. 1096.
798 Bigeleisen, J., Ishida, T., 1973. Application of finite orthogonal polynomials to the thermal functions
799 of harmonic oscillators. V. Isotope chemistry and molecular structure. Simplified theory of end atom
800 isotope effects. Journal of the American Chemical Society 95, 6155-6157.
801 Bouchard, D., Cornaton, F., Hoehener, P., Hunkeler, D., 2011. Analytical modelling of stable isotope
802 fractionation of volatile organic compounds in the unsaturated zone. Journal of Contaminant
803 Hydrology 119, 44-54.
804 Bouchard, D., Hohener, P., Hunkeler, D., 2008a. Carbon Isotope Fractionation During Volatilization of
805 Petroleum Hydrocarbons and Diffusion Across a Porous Medium: A Column Experiment.
806 Environmental Science & Technology 42, 7801-7806.
807 Bouchard, D., Hunkeler, D., Gaganis, P., Aravena, R., Höhener, P., Broholm, M.M., Kjeldsen, P., 2008b.
808 Carbon isotope fractionation during diffusion and biodegradation of petroleum hydrocarbons in the
809 unsaturated zone: Field experiment at Vaerlose airbase, Denmark, and modeling. Environmental
810 Science & Technology 42, 596-601.
811 Bouchard, D., Hunkeler, D., Madsen, E.L., Buscheck, T., Daniels, E.J., Kolhatkar, R., DeRito, C.M.,
812 Aravena, R., Thomson, N., 2018a. Application of Diagnostic Tools to Evaluate Remediation
813 Performance at Petroleum Hydrocarbon-Impacted Sites. Groundwater Monitoring and Remediation
814 38, 88-98.
815 Bouchard, D., Hunkeler, D., Marchesi, M., Aravena, R., Buscheck, T., submitted. Field validation of the
816 solvent-based sampling method to perform compound-specific isotope analysis on gas-phase VOC.
817 submitted to Journal of Contaminant Hydrology.
818 Bouchard, D., Hunkeler, D., Ponsin, V., Aravena, R., Madsen, E.L., Buscheck, T., Kolhatkar, R., Daniels,
819 E.J., Klinchuch, L., Stumpf, P., 2017a. Use of Compound-Specific Isotope Analysis (CSIA) to assess the
820 efficiency of soil vapor extraction applied to a petroleum hydrocarbon source zone. Battelle
821 conference - Fourth International Symposium on Bioremediation and Sustainable Environmental
822 Technologies, Miami, Fl. USA.
823 Bouchard, D., Marchesi, M., Madsen, E.L., Derito, C.M., Thomson, N.T., Aravena, R., Barker, J.F.,
824 Buscheck, T., Kolhatkar, R., Daniels, E.J., Hunkeler, D., 2018b. Diagnostic tools to assess mass removal
825 processes during pulsed air sparging of a petroleum hydrocarbon source zone. Ground Water
826 Monitoring and Remediation. 38, 29-44.
827 Bouchard, D., McLoughlin, P.W., Hunkeler, D., Pirkle, R.J., 2015. $\delta^{13}C$ and $\delta^{37}Cl$ on Gas-Phase TCE for
828 Source Identification Investigation - Innovative Solvent-Based Sampling Method. Environmental
829 Forensics: Proceedings of the 2014 INEF Conference., 70-81. DOI:10.1039/9781782625070-
830 9781782600070.

Bouchard, D., Wanner, P., Luo, H., McLoughlin, P.W., Henderson, J.K., Pirkle, R.J., Hunkeler, D., 2017b. Optimization of the solvent-based dissolution method to sample volatile organic compound vapors for compound-specific isotope analysis. Journal of chromatography. A 1520, 23-34.
Boulding, J., 1995. Practical handbook of soil, vadose zone, and ground-water contamination. Assessment, prevention, and remediation. Lewis Publisher (Boca Raton - USA).
Broholm, M.M., Christophersen, M., Maier, U., Stenby, E.H., Hohener, P., Kjeldsen, P., 2005. Compositional evolution of the emplaced fuel source in the vadose zone field experiment at airbase Vaerlose, Denmark. Environmental Science & Technology 39, 8251-8263.
Christophersen, M., Broholm, M.M., Mosbaek, H., Karapanagioti, H.K., Burganos, V.N., Kjeldsen, P., 2005. Transport of hydrocarbons from an emplaced fuel source experiment in the vadose zone at Airbase V ae rlose, Denmark. Journal of Contaminant Hydrology 81, 1-33.
Chu, K.H., Mahendra, S., Song, D.L., Conrad, M.E., Alvarez-Cohen, L., 2004. Stable carbon isotope fractionation during aerobic biodegradation of chlorinated ethenes. Environmental Science & Technology 38, 3126-3130.
Clingenpeel, S.R., Moan, J.L., McGrath, D.M., Hungate, B.A., Watwood, M.E., 2012. Stable carbon isotope fractionation in chlorinated ethene degradation by bacteria expressing three toluene oxygenases. Frontiers in microbiology 3, 63.
Coplen, T.B., 2011. Guidelines and recommended terms for expression of stable-isotope-ratio and gas-ratio measurement results. Rapid Communications in Mass Spectrometry 25, 2538-2560.
Cozzarelli, I.M., Bekins, B.A., Baedecker, M.J., Aiken, G.R., Eganhouse, R.P., Tuccillo, M.E., 2001. Progression of natural attenuation processes at a crude-oil spill site: I. Geochemical evolution of the plume. J Contam Hydrol 53, 369-385.
Davis, G.B., Rayner, J.L., Trefry, M.G., Fisher, S.J., Patterson, B.M., 2005. Measurement and Modeling of Temporal Variations in Hydrocarbon Vapor Behavior in a Layered Soil Profile. Vadose Zone Journal 4, 225-239.
Dorer, C., Vogt, C., Kleinsteuber, S., Stams, A.J., Richnow, H.H., 2014. Compound-specific isotope analysis as a tool to characterize biodegradation of ethylbenzene. Environ Sci Technol 48, 9122-9132.
Elsner, M., Zwank, L., Hunkeler, D., Schwarzenbach, R.P., 2005. A new concept linking observable stable isotope fractionation to transformation pathways of organic pollutants. Environmental Science & Technology 39, 6896-6916.
Grathwohl, P., Halm, D., Bonilla, Á., Broholm, M.M., Christophersen, M., Comans, R.N.J., Gaganis, P., Gorostiza, I., Höhener, P., Kjeldsen, P., Sloot, H.v.d., 2003. Guideline for groundwater risk assessment at contaminated sites (GRACOS). Recommendations for the assessment of a potential risk of groundwater pollution originating from a soil contamination in the unsaturated zone.
Höhener, P., Bouchard, D., Hunkeler, D., 2008. Stable isotopes as a tool for monitoring the volatilisation of non-aqueous phase liquids from the unsaturated zone. Advances in Subsurface Pollution of Porous Media. Indicators, Processes and Modelling. ed.: L. Candela, I. Vadillo and F.J. Elorza. Vol 14, p.123-135. CRC Press. Taylor and Francis Group, Boca Raton.
Höhener, P., Dakhel, N., Christophersen, M., Broholm, M., Kjeldsen, P., 2006. Biodegradation of hydrocarbons vapors: Comparison of laboratory studies and field investigations in the vadose zone at the emplaced fuel source experiment, Airbase Vaerløse, Denmark. J Contam Hydrol 88, 337-358.
Horst, A., Lacrampe-Couloume, G., 2020. Isotope fractionation (2H/1H, 13C/12C, 37Cl/35Cl) in trichloromethane and trichloroethene caused by partitioning between gas phase and water. Environmental Science: Processes & Impacts 22, 617-626.
Huybrechts, T., Dewulf, J., Van Craeynest, K., Van Langenhove, H., 2001. Evaluation of tetraglyme for the enrichment and analysis of volatile organic compounds in air. J. Chromatogr. A. 922, 207-218.
Imfeld, G., Kopinke, F.D., Fischer, A., Richnow, H.H., 2014. Carbon and hydrogen isotope fractionation of benzene and toluene during hydrophobic sorption in multistep batch experiments. Chemosphere 107, 454-461.
Jakli, G., Tzias, P., Van Hook, W.A., 1978. Vapor pressure isotope effects in the benzene (B)–cyclohexane (C) system from 5 to 80 °C. I. The pure liquids B-d0,B-d1,ortho-,meta-, and para-B-d2, B-d6,C-d0, and C-d12. II. Excess free energies and isotope effects on excess free energies in the

883 solutions B-h6/B-d6, C-h12/C-d12, B-h6/C-h12, B-d6/C-h12, and B-h6/C-d12. The Journal of Chemical
884 Physics 68, 3177-3190.
885 Jancso, G., 2002. Interpretation of isotope effects on the solubility of gases. Nukleonika 47, S53-S57.
886 Jancso, G., Van Hook, W.A., 1974. Condensed phase isotope effects (Especially vapor-pressure
887 isotope effects). Chemical Reviews 74, 689-750.
888 Jeannottat, S., Hunkeler, D., 2012. Chlorine and Carbon Isotopes Fractionation during Volatilization
889 and Diffusive Transport of Trichloroethene in the Unsaturated Zone. Environmental Science &
890 Technology 46, 3169-3176.
891 Jeannottat, S., Hunkeler, D., 2013. Can Soil Gas VOCs be Related to Groundwater Plumes Based on
892 Their Isotope Signature? Environmental Science & Technology 47, 12115-12122.
893 Johnson, P., Ekre, R., Krajmalnik-Brown, R., Rittman, B., Lundegard, P., Hinchee, R., 2013. Assessment
894 of the Natural Attenuation of NAPL Source Zones and Post-Treatment NAPL Source Zone Residuals.
895 Johnson, P.C., Ettinger, R.A., 1991. Heuristic model for predicting the intrusion rate of contaminant
896 vapors into buildings. Environmental Science & Technology 25, 1445-1452.
897 Julien, M., Nun, P., Robins, R.J., Remaud, G.S., Parinet, J., Höhener, P., 2015a. Insights into
898 Mechanistic Models for Evaporation of Organic Liquids in the Environment Obtained by Position-
899 Specific Carbon Isotope Analysis. Environmental Science & Technology 49, 12782-12788.
900 Julien, M., Nun, P., Robins, R.J., Remaud, G.S., Parinet, J., Höhener, P., 2015b. Insights into
901 Mechanistic Models for Evaporation of Organic Liquids in the Environment Obtained by Position-
902 Specific Carbon Isotope Analysi. Environmental Science & Technology 49, 12782-12788.
903 Kirtland, B.C., Aelion, C.M., Stone, P.A., Hunkeler, D., 2003. Isotopic and geochemical assessment of
904 in situ biodegradation of chlorinated hydrocarbons. Environmental Science & Technology 37, 4205-
905 4212.
906 Kopinke, F.D., Georgi, A., 2017. Comment on Vapor Pressure Isotope Effects in Halogenated Organic
907 Compounds and Alcohols Dissolved in Water. Anal Chem 89, 10637-10638.
908 Kuder, T., Philp, P., Allen, J., 2009. Effects of Volatilization on Carbon and Hydrogen Isotope Ratios of
909 MTBE. Environmental Science & Technology 43, 1763-1768.
910 Kurt, Z., Mack, E.E., Spain, J.C., 2014. Biodegradation of cis-dichloroethene and vinyl chloride in the
911 capillary fringe. Environ Sci Technol 48, 13350-13357.
912 Lacks, D.J., 1995. Origins of molar volume isotope effects in hydrocarbon systems. The Journal of
913 Chemical Physics 103, 5085-5090.
914 Lahvis, M.A., Baehr, A.L., Baker, R.J., 1999. Quantification of aerobic biodegradation and volatilization
915 rates of gasoline hydrocarbons near the water table under natural attenuation conditions. Water
916 Resources Research 35, 753-765.
917 Lundegard, P.D., Johnson, P.C., 2006. Source Zone Natural Attenuation at Petroleum Hydrocarbon
918 Spill Sites—II: Application to a Former Oil Field. Groundwater Monitoring & Remediation 26, 93-106.
919 Mackay, D., Shiu, W.-Y., Shiu, W.-Y., Lee, S.C., 2006. Handbook of Physical-Chemical Properties and
920 Environmental Fate for Organic Chemicals (2nd ed.). CRC Press., Boca Raton.
921 McColl, C.M., Johnson, G.R., Brusseau, M.L., 2008. Evaporative mass transfer behavior of a complex
922 immiscible liquid. Chemosphere 73, 607-613.
923 McHugh, T., Kuder, T., Fiorenza, S., Gorder, K., Dettenmaier, E., Philp, P., 2011. Application of CSIA to
924 Distinguish Between Vapor Intrusion and Indoor Sources of VOCs. Environmental Science &
925 Technology 45, 5952-5958.
926 Molins, S., Mayer, K.U., Amos, R.T., Bekins, B.A., 2010. Vadose zone attenuation of organic
927 compounds at a crude oil spill site - interactions between biogeochemical reactions and
928 multicomponent gas transport. J Contam Hydrol 112, 15-29.
929 Patterson, B.M., Aravena, R., Davis, G.B., Furness, A.J., T.P., B., Bouchard, D., 2013. Multiple lines of
930 evidence to demonstrate vinyl chloride aerobic biodegradation in the vadose zone, and factors
931 controlling rates. Journal of Contaminant Hydrology 153, 69–77.
932 Pham, H.T., Kitsuneduka, M., Hara, J., Suto, K., Inoue, C., 2008. Trichloroethylene Transformation by
933 Natural Mineral Pyrite: The Deciding Role of Oxygen. Environmental Science & Technology 42, 7470-
934 7475.

Ponsin, V., Maier, J., Guelorget, Y., Hunkeler, D., Bouchard, D., Villavicencio, H., Hoehener, P., 2015. Documentation of time-scales for onset of natural attenuation in an aquifer treated by a crude-oil recovery system. Science of the Total Environment 512, 62-73.
Reichardt, C., Welton, T., 2010. Empirical Parameters of Solvent Polarity. Solvents and Solvent Effects in Organic Chemistry. Editors C. Reichardt and T. Welton. Wiley Library, pp. 425-508.
Rivett, M.O., Wealthall, G.P., Dearden, R.A., McAlary, T.A., 2011. Review of unsaturated-zone transport and attenuation of volatile organic compound (VOC) plumes leached from shallow source zones. J Contam Hydrol 123, 130-156.
Schaefer, C.E., Ho, P., Berns, E., Werth, C., 2018. Mechanisms for Abiotic Dechlorination of Trichloroethene by Ferrous Minerals under Oxic and Anoxic Conditions in Natural Sediments. Environmental Science & Technology 52, 13747-13755.
Scott, K.M., Lu, X., Cavanaugh, C.M., Liu, J.S., 2004. Optimal methods for estimating kinetic isotope effects from different forms of the Rayleigh distillation equation. Geochimica Et Cosmochimica Acta 68, 433-442.
Sihota, N.J., Trost, J.J., Bekins, B.A., Berg, A., Delin, G.N., Mason, B., Warren, E., Mayer, K.U., 2016. Seasonal Variability in Vadose Zone Biodegradation at a Crude Oil Pipeline Rupture Site. Vadose Zone Journal 15, vzj2015.2009.0125.
Van Hook, A.W., 2006. Condensed matter isotope effect. . in: Kohen, A., Limbach, H.-H. (Eds.). In Isotope effect in Chemistry and Biology. Taylor & Francis group, Boca-Raton.
Verginelli, I., Capobianco, O., Baciocchi, R., 2016. Role of the source to building lateral separation distance in petroleum vapor intrusion. J Contam Hydrol 189, 58-67.
Wade, D., 1999. Deuterium isotope effect on noncovalent interactions between molecules. Chemico-Biological Interactions 117, 191-217.
Wang, G.H., Reckhorn, S.B.F., Grathwohl, P., 2003. Volatile Organic Compounds Volatilization from Multicomponent Organic Liquids and Diffusion in Unsaturated Porous Media. Vadose Zone Journal 2, 692-701.
Wolfsberg, M.W., Hook, A., Paneth, P., Rebelo, L., 2010. Condensed Phase Isotope Effect: Isotope Effects. Isotope Effects in the Chemical, Geological, and Bio Sciences. Springer, Dordrecht, Heidelberg, London, New-York, p. 466.
Zamane, S., Gori, D., Höhener, P., 2020. Multistep partitioning causes significant stable carbon and hydrogen isotope effects during volatilization of toluene and propan-2-ol from unsaturated sandy aquifer sediment. Chemosphere 251, 126345.

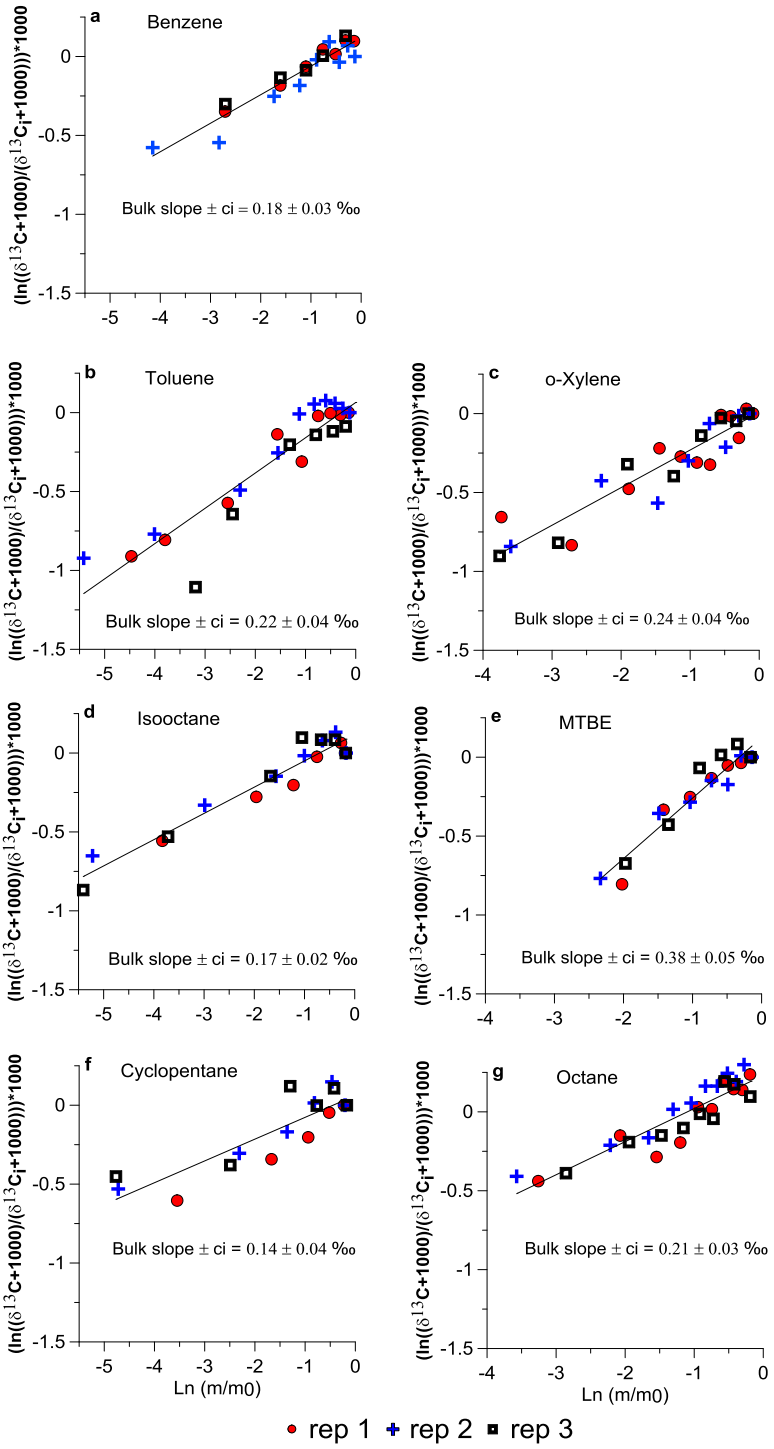

969

970 **Figure 1:** Carbon isotope fractionation during stepwise air-NAPL vaporization for selected
971 compounds. The change in carbon isotope ratio is plotted as function of the remaining mass (m/m0)
972 in the Ln scale. The bulk slope and the 95% confidence interval (ci) were determined using all plotted
973 data (triplicate experiments). NAPL designates the neat liquid of each compound.

974

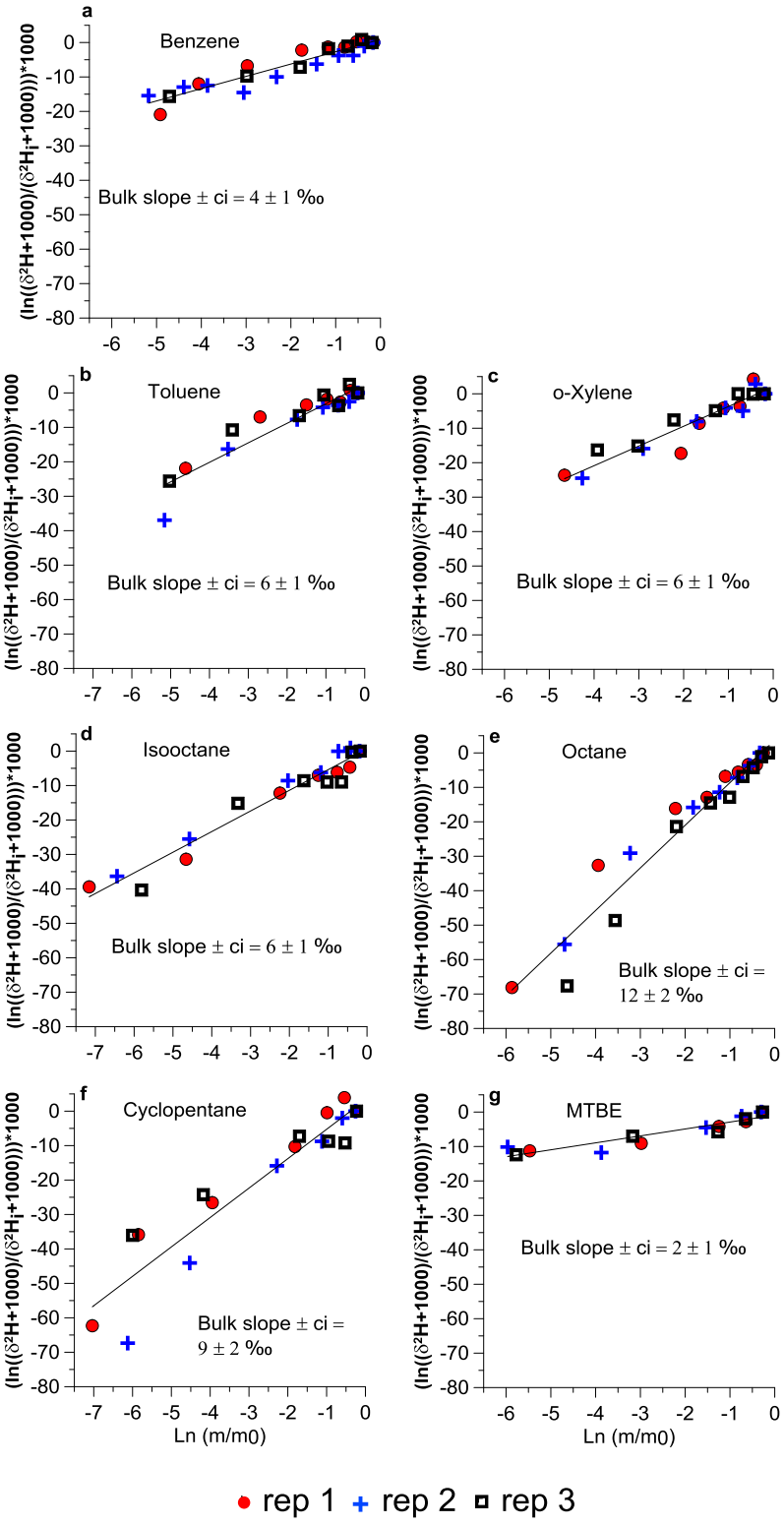

Figure 2: Hydrogen isotope fractionation during stepwise air-NAPL vaporization for selected compounds. The change in hydrogen isotope ratio is plotted as function of the remaining mass (m/m0) in the Ln scale. The bulk slope and the 95% confidence interval (ci) were determined using all plotted data (triplicate experiments). NAPL designates the neat liquid of each compound.

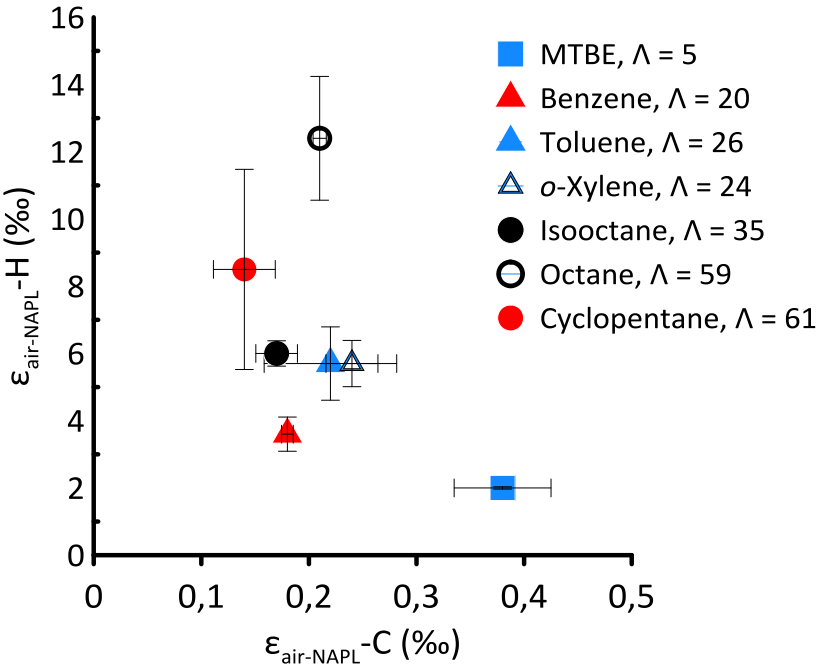

980

981 **Figure 3:** Plot of H-$\varepsilon_{air\text{-}NAPL}$ as function of C-$\varepsilon_{air\text{-}NAPL}$ measured for monoaromatic (BT*o*-X) aliphatic (*n*-
982 octane, isooctane and cyclopentane) and fuel oxygenate (MTBE) compounds caused by air-NAPL
983 vaporization. The Λ values reported represent H-ε / C-ε ratios.

984

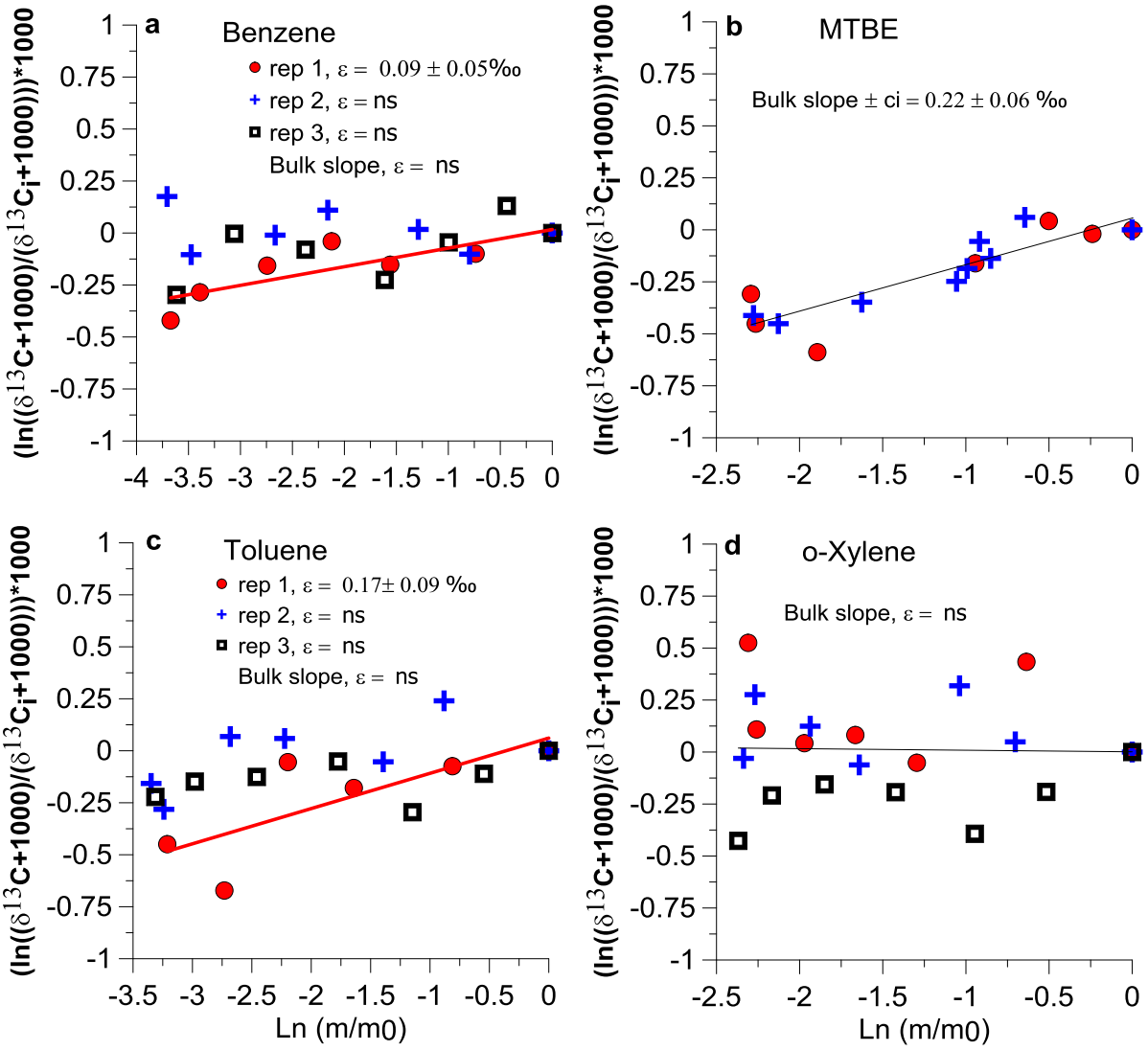

Figure 4: Carbon isotope fractionation during stepwise air-water partitioning for selected compounds. The change in carbon isotope ratio is plotted as function of the remaining mass (m/m0) in the Ln scale. The bulk slope (black line) and the 95 % confidence interval (ci) were determined using all plotted data (triplicate experiments), except for MTBE (duplicate experiments). Replicate-specific slope is represented by a red line. ns: not significant.

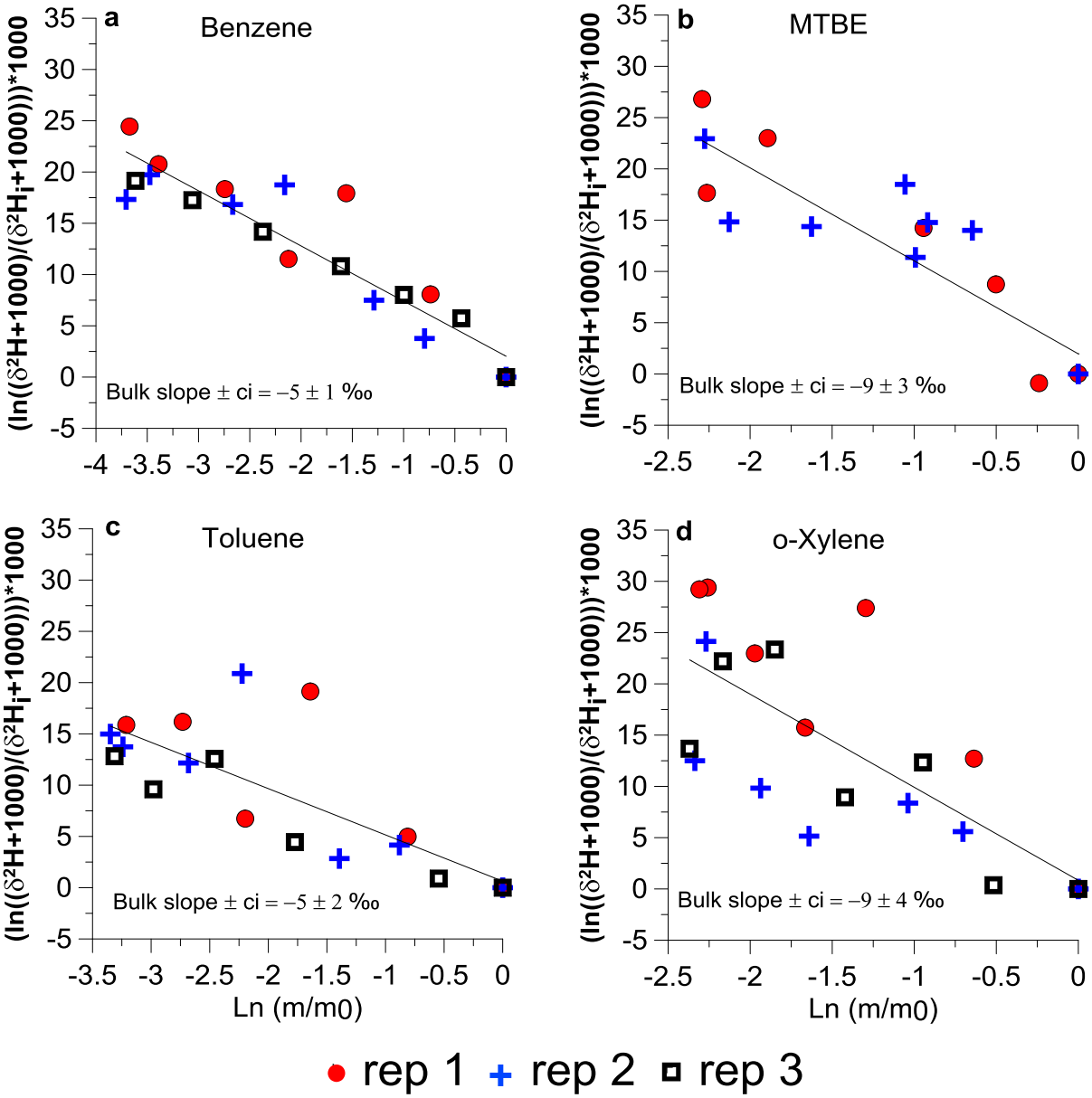

992

993 **Figure 5:** Hydrogen isotope fractionation during stepwise air-water partitioning for selected
994 compounds. The change in hydrogen isotope ratio is plotted as function of the remaining mass
995 (m/m0) in the Ln scale. The bulk slope and the 95 % confidence interval (ci) were determined using
996 all plotted data (triplicate experiments), except for MTBE (duplicate experiments).

997

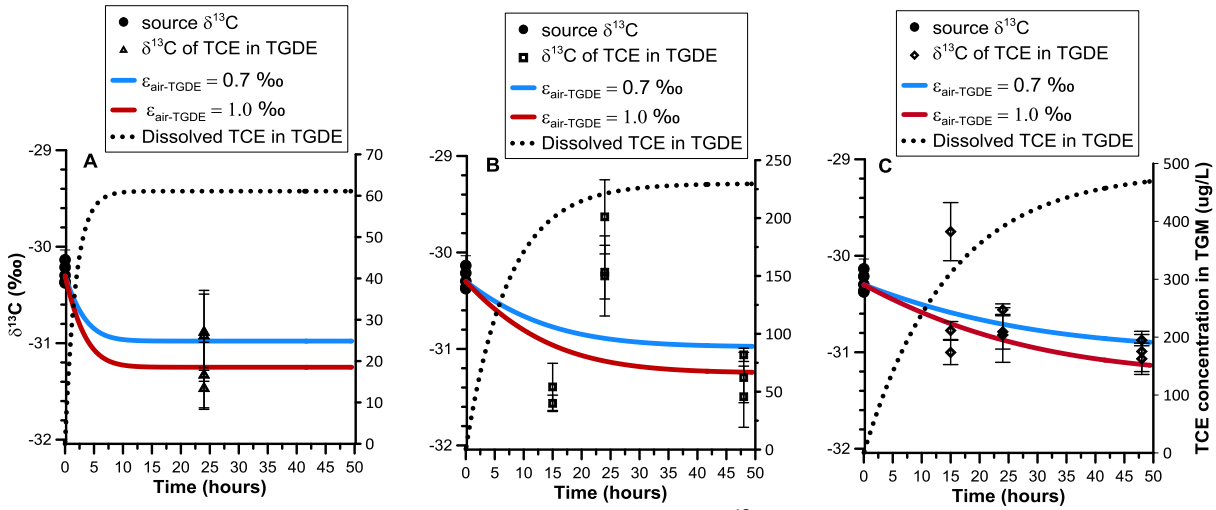

Figure 6: Evolution of concentrations (black line) and $\delta^{13}C$ composition (blue and red lines, considering different isotope enrichment factors $\varepsilon_{air\text{-}TGDE}$) for TCE dissolved in TGDE during 3 simulated gas-phase sampling events using TCE gas-phase concentration of 21 µg/m^3 (A), 79 µg/m^3 (B), and 167 µg/m^3 (C), and respective gas flow rate of 800, 400 and 200 mL/minute. Laboratory data from Bouchard et al. (2017b)

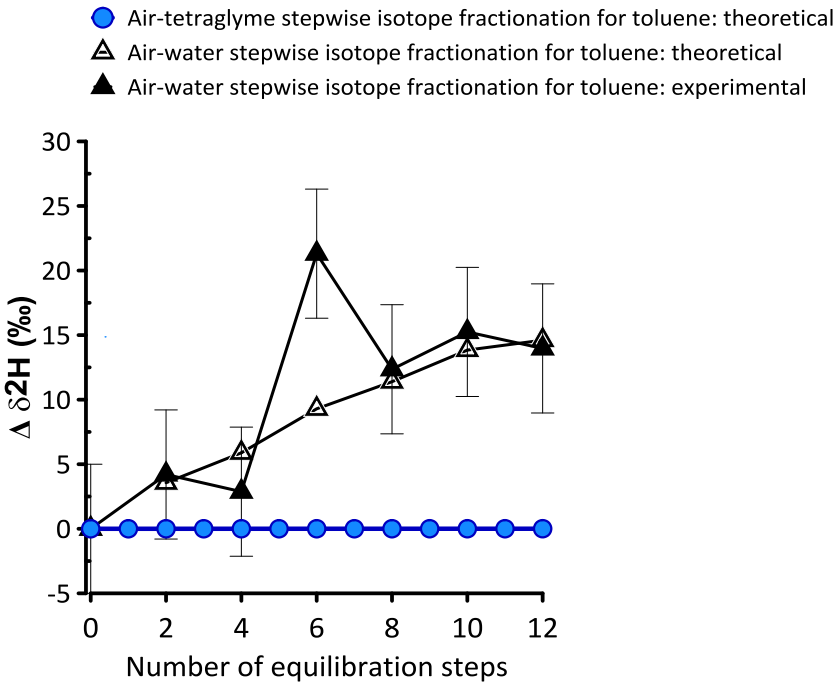

Figure 7: δ^2H composition for remaining toluene in the liquid after 12 mass removal steps from a closed system caused by air-water partitioning (triangles) and by air-TGDE partitioning (circles).